A competitive binding assay for RNA ligand discovery

Wintermans, S.E.L.

THE PSEUDOKNOT

Chapter 3

High-throughput screening and hit validation for the $PreQ_1$ riboswitch

Parts of this chapter have been published in:

S.E.L. Wintermans, J.S. Hoffmann, V. van Kuijk, Y. Durmus, M.D. Tacoma, I. Broekhuizen, A.P.A. Janssen, H. van den Elst, B.R. van Doodewaerd, P.P. Geurink, M.E. Artola, R.C.L. Olsthoorn. *High-Throughput Competitive Binding Assay for Targeting RNA Tertiary Structures with Small Molecules: Application to Pseudoknots and G-Quadruplexes*. Nucleic Acids Research, (2025), *53* (16).

Introduction

Antibiotic resistance is one of the top threats to human health according to the World Health Organization, and development of antibiotics with new modes-of-action should be a priority for future drug development projects. Riboswitches have been widely regarded as potential antibiotic targets since their discovery at the start of this millennium[1,2]. Thought to be remnants of a time when RNA regulated everything[3], riboswitches are RNA structures in the 5′-untranslated region (5′-UTR) of bacterial mRNA that can regulate gene expression independently of proteins, by binding to a ligand that drives the RNA to undergo a conformational change. This switch in structure directly leads to a change in gene expression, for example by terminating transcription of the downstream mRNA or by preventing translation through sequestration of the Shine-Dalgarno (SD) sequence. Riboswitches regulate many essential cellular processes and biosynthetic pathways and are present and highly conserved in many different bacteria, making them interesting potential antibiotic targets[4,5].

The $PreQ_1$ riboswitch is a promising and unique target for antibiotic development, as it is a regulatory RNA structure involved in the biosynthesis pathway of the essential modified nucleobase Queuosine (Q), which is important for bacterial virulence and viability. In particular, this riboswitch regulates the synthesis and transport of $PreQ_1$, one of the key precursors of Q. Q is a hypermodified nucleobase in various tRNAs that is necessary for correct decoding of mRNA. Absence of Q can lead to dysregulation of cellular functions, and in the case of bacteria can lead to decreased viability and virulence[6–8]. Upon binding of $PreQ_1$, the riboswitch downregulates the expression of four enzymes (QueCDEF) involved in the biosynthesis of $PreQ_1$ and two proteins (QueT and YhhQ) involved in the transport of $PreQ_1$[9–12]. Due to its important regulatory role in the biosynthesis of Q, a process that only occurs in bacteria, the $PreQ_1$ riboswitch is considered to be an interesting target for antibiotic drug development. A potential strategy to interfere with the biological function of the $PreQ_1$ riboswitch is to find an artificial ligand that binds the riboswitch, represses gene expression and ultimately prevents Q synthesis. For finding such ligands, it is important to consider the architecture of different $PreQ_1$ riboswitches.

The $PreQ_1$ riboswitch family consists of three classes ($PreQ_1$-I, II and III), each class with distinct structures and functions (**Figure 3.1**). $PreQ_1$-I riboswitches are the smallest and most abundant class of all $PreQ_1$ riboswitches[13,14]. $PreQ_1$ binds to the riboswitch by, in part, forming a *cis* Watson-Crick-Franklin (WCF) base pair with a conserved cytosine,

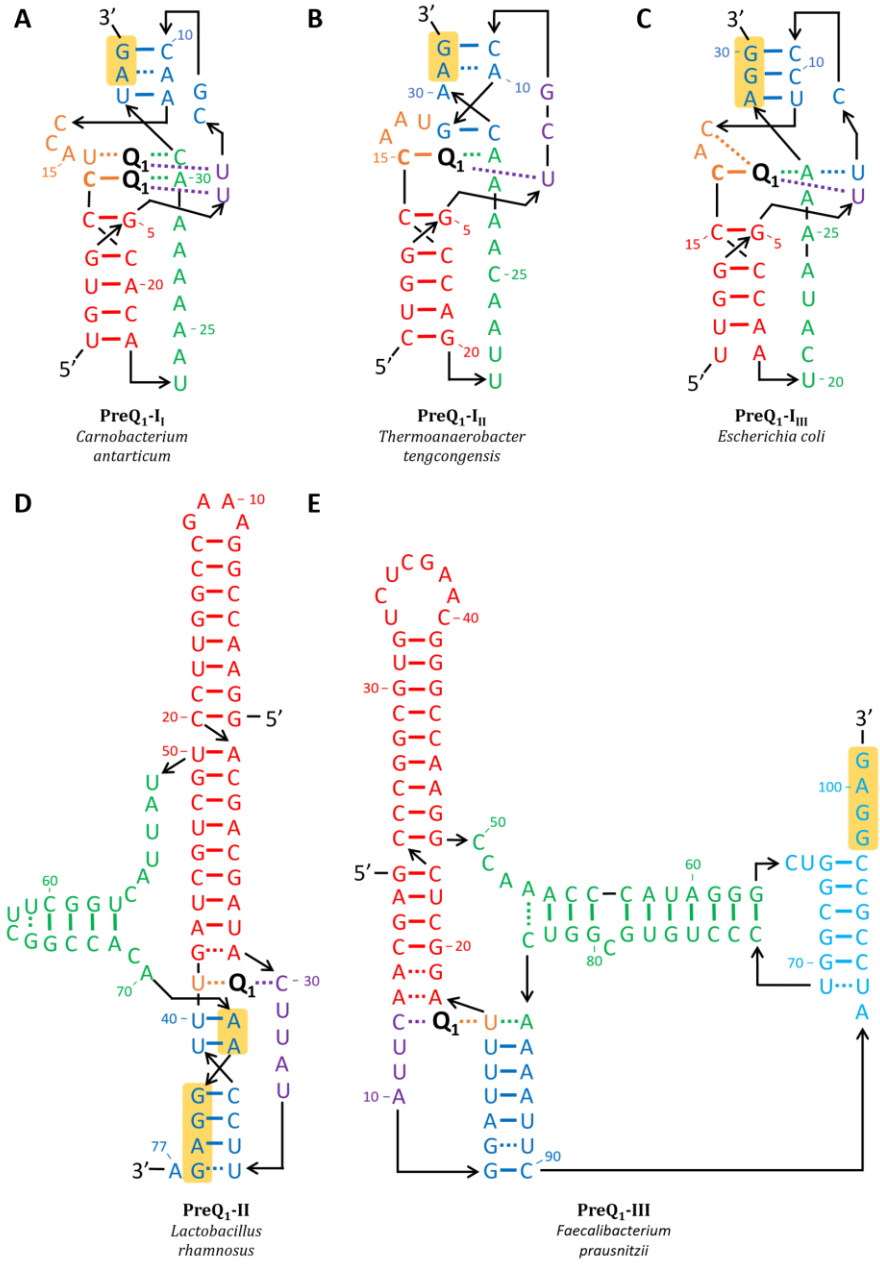

Figure 3.1. 2D structures of representative class I, II and III $PreQ_1$ riboswitches in their $PreQ_1$ (Q_1)-bound state. **A-C)** Class I $PreQ_1$ ($PreQ_1$-I) riboswitches. Representative sequences from three types are shown: $PreQ_1$-I_I from *Carnobacterium antarticum* (**A**), $PreQ_1$-I_{II} from *Thermoanaerobacter tengcongensis* (**B**) and $PreQ_1$-I_{III} from *Escherichia coli* (**C**). **D)** Class II $PreQ_1$ ($PreQ_1$-II) riboswitch from *Lactobacillus rhamnosus*. **E)** Class III $PreQ_1$ ($PreQ_1$-III) riboswitch from *Faecalibacterium prausnitzii*. Full lines denote Watson-Crick-Franklin (WCF) base-pairs, dashed lines denote non-WCF base-pairs. For simplicity, not all tertiary interactions are shown. The Shine-Dalgarno sequence is highlighted in yellow.

which leads to the formation of a hairpin (H)-type pseudoknot. This conformational switch results in downregulation in the expression of QueCDEF, QueT or YhhQ. For the $PreQ_1$-I riboswitches, three different subgroups with varying aptamer consensus models are recognized. Class I type I $PreQ_1$ riboswitches (abbreviated $PreQ_1$-I_I) (**Figure 3.1A**) regulate both QueCDEF expression through transcription termination, and QueT expression through translation prevention[9]. Interestingly, $PreQ_1$-I_I riboswitches bind two $PreQ_1$ ligands in the same pocket, which was first observed with the *Carnobacterium antarticum* $PreQ_1$-I_I riboswitch[15]. Class I type II $PreQ_1$ riboswitches ($PreQ_1$-I_{II}, **Figure 3.1B**) also regulate transcription and translation of QueCDEF and QueT, although they bind $PreQ_1$ in a 1:1 stoichiometry. The $PreQ_1$-I_{II} riboswitches from *Bacillus subtilis* and *Theromanaerobacter tengcongensis* were the first $PreQ_1$ riboswitches to have their structure determined through NMR and crystallography[16–18]. Class I type III $PreQ_1$ riboswitches ($PreQ_1$-I_{III}, **Figure 3.1C**) were discovered last, and are known to regulate the expression of the $PreQ_0$/$PreQ_1$ dual transporter YhhQ through a translation prevention mechanism[14,19]. A co-crystal structure of the $PreQ_1$-I_{III} *Escherichia coli* riboswitch confirmed a 1:1 $PreQ_1$ binding stoichiometry[20].

Class II $PreQ_1$ riboswitches ($PreQ_1$-II, **Figure 3.1D**) are about twice as large as $PreQ_1$-I riboswitches and form an HL_{out} pseudoknot. They exclusively regulate translation of the $PreQ_1$ transporter QueT by sequestering the entire SD sequence[21]. $PreQ_1$-II riboswitches bind to $PreQ_1$ with a conserved cytosine through a *trans* WCF base-pair in a 1:1 stoichiometry. The most recently discovered class III $PreQ_1$ riboswitches ($PreQ_1$-III, **Figure 3.1E**) are the largest and most complex of all $PreQ_1$ riboswitch classes. Their structure is thought to form a double pseudoknot structure: a H-type pseudoknot that is nested within a HL_{out} pseudoknot[21]. $PreQ_1$-III riboswitches are known to be involved in regulation of QueT, although their mechanism of gene regulation is not fully characterized yet.

The large variation in $PreQ_1$ riboswitch architecture makes the design of general $PreQ_1$ riboswitch ligands extremely challenging. Most efforts for finding new $PreQ_1$ riboswitch ligands have been geared towards $PreQ_1$-I riboswitches, as they are the most abundant and well-characterized class. Both modification of $PreQ_1$ and high-throughput screening (HTS) campaigns for finding synthetic ligands have been reported. In the first paper to report a $PreQ_1$ riboswitch, now known to be the $PreQ_1$-I_{II} riboswitch from *Bacillus subtilis* (*Bsu*), apparent binding affinities of $PreQ_1$ and twelve analogues were determined (**Figure 3.2A**)[9].

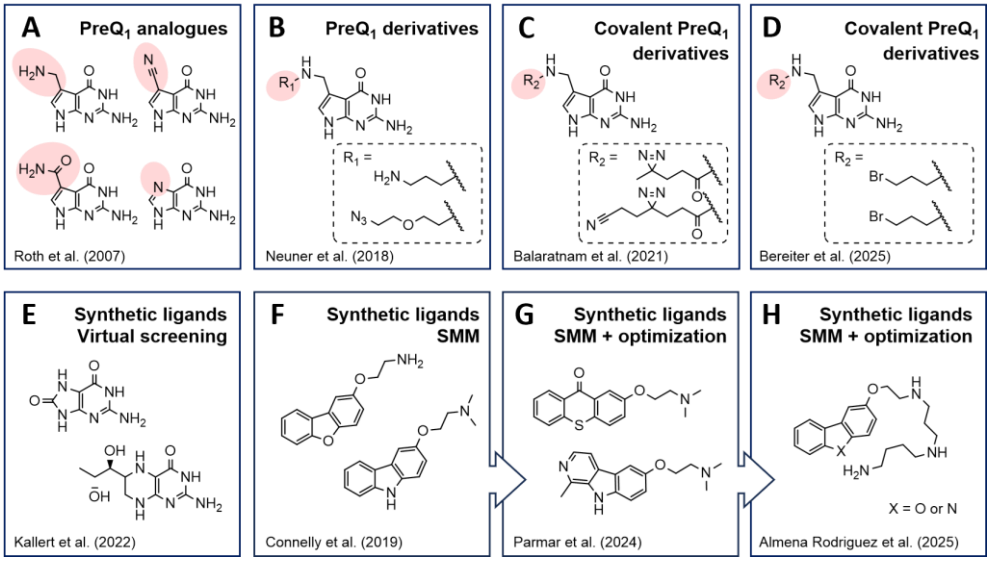

Figure 3.2. Overview of reported ligands for the $PreQ_1$ riboswitch, including (**A**) $PreQ_1$ analogues, (**B**) $PreQ_1$ derivatives, (**C-D**) covalent $PreQ_1$ derivatives, (**E**) synthetic ligands found by a small molecule microarray (SMM) screening, (**F**) synthetic ligands found by virtual screening and (**G-H**) ligands found by virtual optimisation of the hits from the SMM screening. Pink shading indicates variation from $PreQ_1$.

Nearly a decade later, it was shown that installing aminoalkyl- and azidoalkyl-modifications on the aminomethyl group of $PreQ_1$ molecules is tolerated by the $PreQ_1$-I_{II} *Thermoanaerobacter tengcongensis* (*Tte*) and $PreQ_1$-II *Streptococcus pneumoniae* (*Spn*) riboswitches, although only the azido-alkyl functionalization retained *in vivo* gene regulation activity (**Figure 3.2B**)[22]. Moreover, a striking discrepancy between *in vitro* affinity, *in vitro* binding kinetics and *in vivo* gene regulation activity was observed. Further efforts to functionalize the $PreQ_1$ aminomethyl group with electrophilic or photo-crosslinking covalent probes (**Figure 3.2C**) confirmed that modification of the aminomethyl group does not interfere with the ligand binding mode, although binding affinity to the *Tte* and *Bsu* $PreQ_1$-I_{II} riboswitches is reduced approximately 50-fold and transcription termination activity with the *Staphylococcus saprophyticus* (*Ssa*) $PreQ_1$-I_{II} riboswitch is reduced 1000-fold[23]. Installing primary alkyl halides with a carefully selected alkyl chain length on the aminomethyl group (**Figure 3.2D**) to covalently bind a nearby guanine in the $PreQ_1$ binding pocket also proved to be an efficient crosslinking strategy[24,25].

Besides modification of the cognate ligand, HTS campaigns to find synthetic ligands for $PreQ_1$ riboswitches have also been performed. A virtual screening with a library of 12,507 compounds against the *Bsu* $PreQ_1$-I_{II} riboswitch identified several guanine-like hits, whose binding was confirmed with microscale thermophoresis (MST) (**Figure 3.2E**)[26]. Reported binding affinities ranged from mid-nanomolar to mid-micromolar concentrations. Unfortunately, the identified hits were not tested in gene regulation assays. A small molecule microarray (SMM) screening was also carried out with the *Bsu* $PreQ_1$-I_{II} riboswitch, in which fluorescently labelled target RNA was added to ligands that were covalently linked to a surface (**Figure 3.2F**)[27]. From a library of 26,227 compounds, the best hit bound selectively to the *Bsu* and *Tte* $PreQ_1$-I_{II} riboswitches in sub-micromolar concentrations and was able to regulate *in vitro* transcription termination of the *Ssa* $PreQ_1$-I_{II} riboswitch at high micromolar concentrations. Subsequent virtual optimisation of the best SMM hit resulted in the identification of a ligand able to modulate gene regulation *in vitro* and *in vivo* (**Figure 3.2G**)[28]. Finally, installing positively charged handles on the best SMM hit did not improve binding affinity (**Figure 3.2H**)[29].

While the efforts to modify $PreQ_1$ and screen for synthetic ligands proved that development of new $PreQ_1$ riboswitch ligands holds potential, none of the reported compounds have been evaluated for antibacterial activity. Therefore, the discovery of new $PreQ_1$ riboswitch ligands for antibiotic drug development remains an interesting field of research. To find new ligands that can regulate gene expression through stabilization of the pseudoknot conformation of this dynamic RNA tertiary structure, a competitive binding antisense assay (CB ASsay) was developed (see Chapter 2). This assay was applied to the *Fusobacterium nucleatum* (*Fnu*), *Tte* and *Bsu* $PreQ_1$-I_{II} riboswitches and to the *Enterococcus faecalis* (*Efa*) $PreQ_1$-I_I riboswitch. Moreover, complimentary functional assays for hit validation were developed with the *Fnu*, *Tte*, *Bsu* $PreQ_1$-I_{II} riboswitches and the *Escherichia coli* (*Eco*) $PreQ_1$-I_{III} riboswitch.

In this Chapter, the CB ASsay was adapted into a HTS format and a HTS was performed with the *Fnu* $PreQ_1$-I_{II} riboswitch. Four *Fnu* riboswitch-binding molecules were identified, which were subsequently tested with the *Tte*, *Bsu* and *Efa* riboswitches, evaluated in functional assays with the *Fnu*, *Bsu*, *Tte* and *Eco* riboswitches, and docked using the known crystal structure of the *Bsu* and *Tte* riboswitches to identify possible binding modes. For the most promising hit, a small library of analogues was synthesized and tested in both CB ASsays and functional assays.

Results

The CB ASsay developed in Chapter 2 was adapted into a high-throughput screening (HTS) format for the screening of potential ligands targeting the clinically relevant *Fusobacterium nucleatum* (*Fnu*) $PreQ_1$-I_{II} riboswitch. A commercially available RNA-focused library from Enamine, comprising 15,520 RNA-binding compounds, was screened in duplicate at a final ligand concentration of 25 µM. Positive and negative controls were established using an excess of unlabelled antisense oligonucleotide (ASO) and DMSO, respectively (**Figure S3.1A and S3.1B**). For additional quality control, 25 µM $PreQ_1$ and guanine were screened alongside the compounds. The HTS data were analysed with KNIME Analytics Platform. Z'-scores were calculated for every plate and ranged from 0.764 to 0.969, with an average Z'-score of 0.815, indicating that the assay was of high quality with a good distinction between positive and negative signals.

Raw fluorescence data (**Figure S3.1C and S3.1D**) were normalized to account for plate, row and column, minimizing potential plate effects[33]. The resulting 'B-scores' of both screenings are shown in **Figure 3.3A**. Unfortunately, the 'strongest' hits from either the first or second screening did not completely overlap. Therefore, 107 initial hits were identified based on the following criteria: compounds exhibiting high activity (B-score >10) in one of the single screenings and compounds displaying moderate activity (B-score 5 - 10) in both screenings. The 107 initial hits, along with 136 of their most active analogues, underwent a duplicate screening at 100 µM (**Figure 3.3B**). To minimize the chance of false negatives, both the confirmed hits and initial hits were re-tested at 5, 25, 50 and 100 µM, resulting in 21 promising hits (**Table S3.4, Figure S3.2**). Among these, based on displayed activity and distinctiveness of the molecular structure, the nine most promising compounds were selected for re-purchase and further evaluation. Initial CB ASsays revealed five false positives, with one compound showing no activity and four displaying nonspecific enhancement of Cy5 signal due to visible insolubility[34].

The four selected hits (**Figure 3.3C**) present typical drug-like properties[35], with an average molecular weight of 323.1 Da, 1.8 H-bond donors, 4.8 H-bond acceptors, 3.5 rotatable bonds and a calculated octanol-water partition coefficient (cLogP) of 2.39. The total hit rate was 0.03%, which is in line with typical hit rates found for RNA targeting HTS campaigns[36,37]. For the four hits, the concentration at which the ligand inhibits ASO binding by 50% (apparent half-maximal effective concentration, EC_{50}) was determined using both the WT* and C17U mutant *Fnu* $PreQ_1$ riboswitch (**Figure 3.4A, 3.4B and Table 3.1**). All hits exhibited competitive binding activity only at high ligand

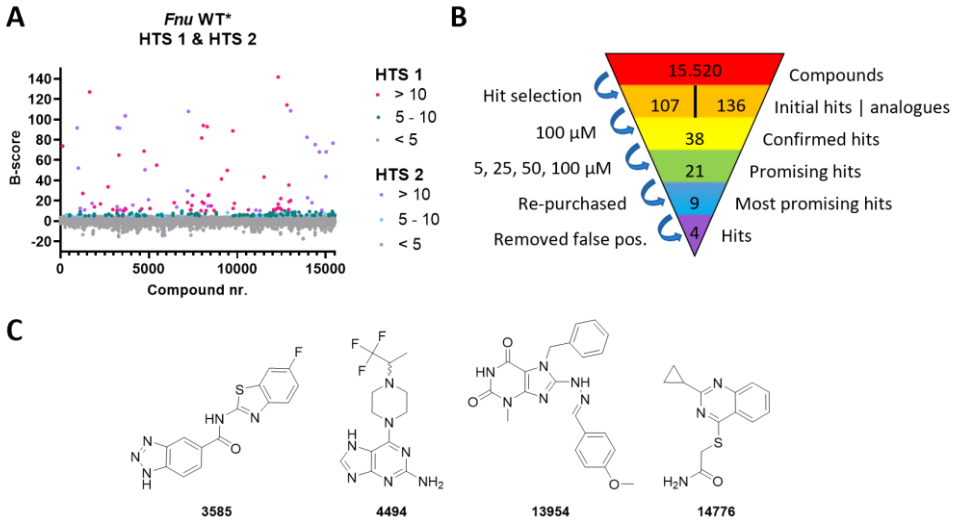

Figure 3.3. Results of the high-throughput screening (HTS) of the Enamine RNA-focused library against the wildtype* (WT*) *Fusobacterium nucleatum* (*Fnu*) $PreQ_1$-I_{II} riboswitch with the competitive binding antisense assay (CB ASsay). **A)** Calculated B-scores for all screened compounds in both high-throughput screenings. High activity hits (B-score >10) are indicated in pink (HTS 1) or purple (HTS 2), moderate activity hits (B-score = 5–10) in green (HTS 1) or blue (HTS 2), inactive compounds (B-score <5) in grey. **B)** Workflow of hit selection and confirmation. **C)** Chemical structures of the four identified hits for the *Fnu* riboswitch: **3585**, **4494**, **13954** and **14776**.

concentrations (EC_{50} >100 µM) for both the WT* and mutant *Fnu* $PreQ_1$-I_{II} riboswitches. Unfortunately, screening of higher ligand concentrations was limited by the solubility of the compounds in the aqueous buffer. Compound **4494**, the only compound soluble at millimolar concentrations, showed a decrease in CB activity for the C17U mutant *Fnu* $PreQ_1$-I_{II} riboswitch, suggesting an interaction with this nucleobase and thus a similar binding mode as $PreQ_1$.

To assess whether ligand binding induces pseudoknot (PK) formation, the CB ASsay was visualized with native PAGE (**Figure 3.4C**). Only **4494** demonstrated a clear dose-dependent competition with the ASO (EC_{50} = 446 µM). While both **3585** and **14776** displayed a more prominent PK band at higher ligand concentrations, it remains unclear whether they promote ligand-induced PK formation as **3585** shows an unlikely, rapid turning point for PK formation and **14776** is a highly coloured compound that quenches fluorescent signal at high concentrations and thus interferes with the read-out. Further assessments with assays that do not rely on fluorescence may provide more insight into their binding behaviour. Unfortunately, compound **13954** did not promote PK formation on native gel.

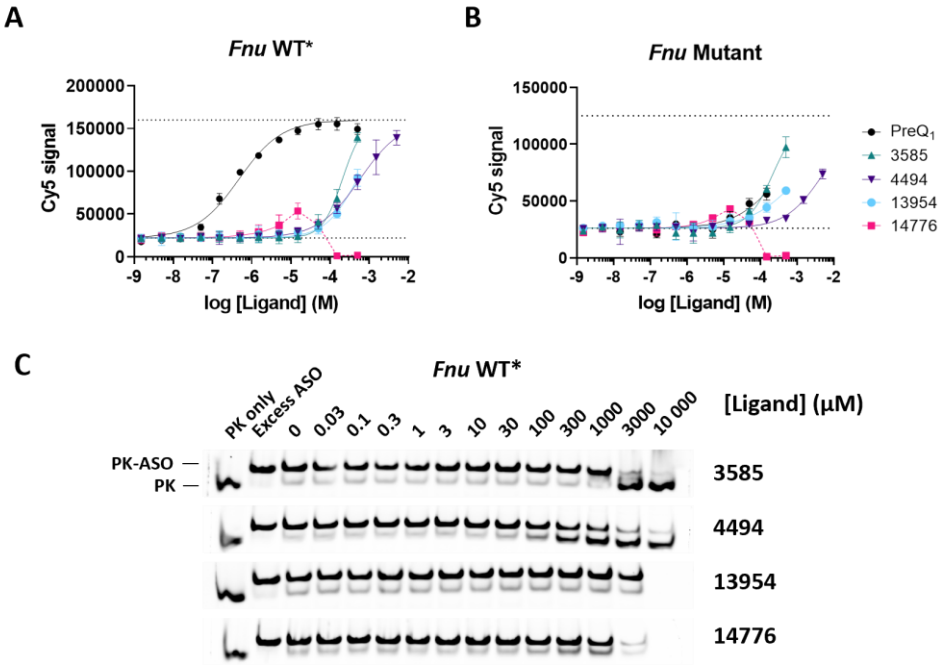

Figure 3.4. Hit validation of identified hits. **A-B)** Competitive binding antisense assay (CB ASsay) of identified hits for the *Fusobacterium nucleatum* (*Fnu*) wildtype* (WT*) (**A**) and *Fnu* mutant $PreQ_1$-I_{II} riboswitch (**B**). Dotted lines denote the minimum and maximum Cy5 signal as determined by the positive and negative controls. **C)** CB ASsay with the *Fnu* WT* $PreQ_1$-I_{II} riboswitch visualized on native PAGE. Cy5-labelled pseudoknot (PK) (1 eq.) was pre-incubated with ligand, after which unlabelled antisense oligonucleotide (ASO) (1 eq.) was added, and the two possible conformations (PK-ligand and PK-ASO) were separated on a 20% (w/v) polyacrylamide gel. All measurements were performed in duplicate.

Table 3.1. Overview of EC_{50} values from the competitive binding antisense assay (CB ASsay) of the identified hits, as determined for the *Fusobacterium nucleatum* (*Fnu*) wildtype* (WT*), the *Thermoanaerobacter tengcongensis* (*Tte*), *Bacillus subtilis* (*Bsu*) and *Enterococcus faecalis* (*Efa*) WT and *Fnu* C17U mutant $PreQ_1$-I riboswitches. n.d. = not determined due to compound interference. ndb = no detectable binding

	Fnu		***Tte***	***Bsu***	***Efa***
	WT*	**Mutant**	**WT**	**WT**	**WT**
	EC_{50} (µM) CB ASsay	**EC_{50} (µM)** CB ASsay	**EC_{50} (µM)** CB ASsay	**EC_{50} (µM)** CB ASsay	**EC_{50} (µM)** CB ASsay
3585	207 ± 23.2	215 ± 38.3	202 ± 110	77.7 ± 33.0	542 ± 44.7
4494	579 ± 75.3	4981 ± 1239	10.7 ± 1.60	2503 ± 881.0	4282 ± 1037
13954	495 ± 91.7	>500	~ 155	171 ± 81.9	144 ± 23.2
14776	n.d.	n.d.	ndb	ndb	ndb

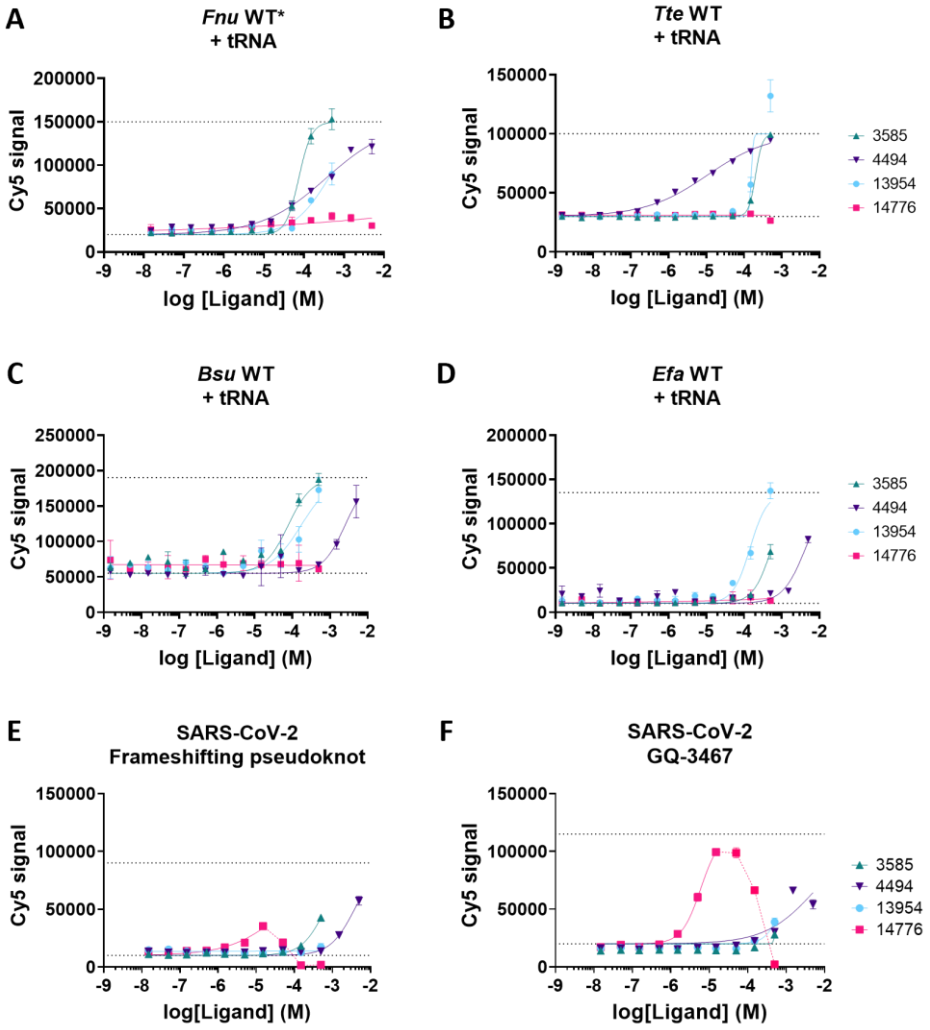

Figure 3.5. Hit selectivity of identified hits. **A-D)** Competitive binding antisense assay (CB ASsay) of identified hits, with the *Fusobacterium nucleatum* (*Fnu*) wildtype* (WT*) PreQ$_1$-I riboswitches with tRNA (**A**), *Thermoanaerobacter tengcongensis* (*Tte*) WT with tRNA (**B**), *Bacillus subtilis* (*Bsu*) WT with tRNA (**C**) and *Enterococcus faecalis* (*Efa*) WT with tRNA (**D**). **E-F)** CB ASsay of identified hits with the SARS-CoV-2 frameshifting pseudoknot (**E**) and a SARS-CoV-2 G-quadruplex (GQ-3467) (**F**). Dotted lines denote the minimum and maximum Cy5 signal as determined by the positive and negative controls. All measurements were performed in duplicate.

To determine the selectivity of the hit compounds, the CB ASsay was also conducted in the presence of a 2000-fold excess of tRNA from yeast (**Figure 3.5A**). Addition of tRNA did not decrease the CB activity of **3585**, **4494** and **13954**, indicating that they do not bind unselectively to structured RNA. However, the CB activity of **14776** did diminish in the presence of tRNA, indicating unspecific binding. Intriguingly, tRNA also reduced the quenching effect of **14776** at high concentrations.

The binding to different $PreQ_1$-I riboswitches was subsequently assessed with the *Thermoanaerobacter tengcongensis* (*Tte*) and *Bacillus subtilis* (*Bsu*) $PreQ_1$-I_{II} riboswitches and the *Enterococcus faecalis* (*Efa*) $PreQ_1$-I_I riboswitch (**Figure 3.5B-D, Table 3.1**). To avoid unspecific binding and fluorescence interference, the CB ASsay was performed in the presence of tRNA. Compounds **3585** and **13954** displayed a high micromolar EC_{50} for all $PreQ_1$-I riboswitches, with only slight variations in activity between sequences. In contrast, observed ligand activity of compound **4494** varied greatly between different riboswitches. Notably, **4494** showed significantly higher activity for the *Tte* riboswitch (EC_{50} = 10.7± 1.60 µM) compared to *Fnu*, *Bsu* and *Efa*. Because of this, competitive binding of the hits to the *Tte* PK was also evaluated on native gel (**Figure S3.3**), which confirmed that **4494** showed significant competitive binding.

Further selectivity tests were performed with two RNA structures from the SARS-CoV-2 genome: a frameshifting PK (see Chapter 4) and a G-quadruplex (GQ-3467, see Chapter 5) (**Figure 3.5E and 3.5F**). Unspecific binding by **14776** was observed with both the frameshifting PK and particularly with GQ-3467, as it competes with their labelled ASOs at mid-micromolar concentrations. Compounds **3585** and **4494** also exhibit some competitive binding activity with the SARS-CoV-2 structures, although only at millimolar concentrations.

Functional assays

To further evaluate the riboswitch ligands, $PreQ_1$ and the four hits were tested in functional assays, including frameshift and translation prevention assays. Frameshift assays measure the increase in –1 ribosomal frameshifting (–1 FS) that is caused by ligand-induced formation and/or stabilization of an RNA tertiary structure. To evaluate the binding of the hits to different $PreQ_1$-I riboswitches, FS assays were carried out with the *Fnu*, *Bsu*, *Tte* and *Escherichia coli* (*Eco*) sequences (**Figure 3.6**). Compound **4494** was the only hit that clearly enhanced frameshifting with the *Tte* riboswitch and, to a lesser degree, the *Eco* riboswitch, thus demonstrating its affinity to these riboswitches and its capacity to stabilize the pseudoknot structure. Compared to the structure of the *Bsu* and *Eco* riboswitches, the *Tte* riboswitch has a relatively accessible $PreQ_1$ binding site (**Figure S3.4**), which could explain why the large (2,2,2-trifluoro-1-methylethyl)-piperazine group of **4494** is more easily accommodated in the *Tte* structure. Unfortunately, compounds **3585**, **13954** and **14774** do not induce frameshifting.

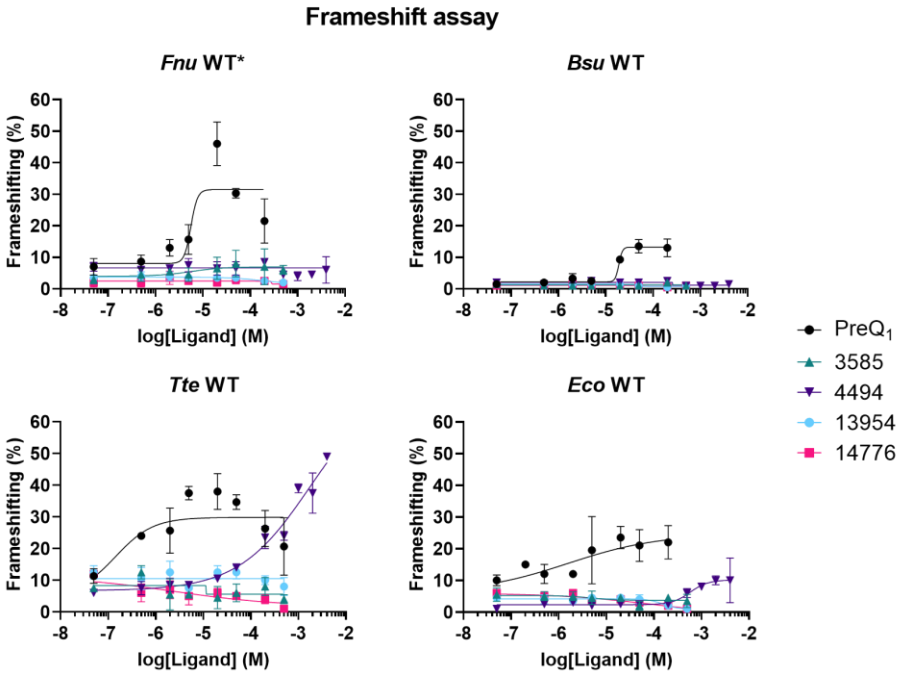

Figure 3.6. Frameshift assays of $PreQ_1$ and hit compounds with the *Fusobacterium nucleatum* (*Fnu*) wildtype* (WT*) (top left), *Bacillus subtilis* (*Bsu*) WT (top right), *Thermoanaerobacter tengcongensis* (*Tte*) WT (bottom left) and *Escherichia coli* (*Eco*) WT (bottom right) $PreQ_1$-I riboswitches. Frameshift percentages were calculated by normalizing the luminescent signal to the in-frame control. Measurements were performed in duplicate.

In the translation prevention assay, the effect of a ligand on the translation of a small reporter peptide under the regulatory control of the *Tte* and *Eco* $PreQ_1$-I riboswitches can be assessed (**Figure 3.7**). As shown in Chapter 2, upon the addition of $PreQ_1$, translation was reduced by 90% for both the WT and C-to-U mutant *Tte* and *Eco* riboswitches, albeit the mutants required a higher concentration of $PreQ_1$ to achieve this effect. Unfortunately, compounds **3585** and **13954** only exhibited translation reduction at millimolar concentrations, which was attributed to general toxicity after testing translation reduction with a fully scrambled *Tte* riboswitch (data not shown). At non-toxic concentrations, compound **14776** showed a decreased translation with the *Eco* WT riboswitch and compound **4494** reduced translation with the *Tte* WT riboswitch. Interestingly, both compounds show a lower activity against mutant riboswitches, suggesting that both **4494** and **14776** can reduce translation through direct interaction with the riboswitch, specifically with the highly conserved cytosine.

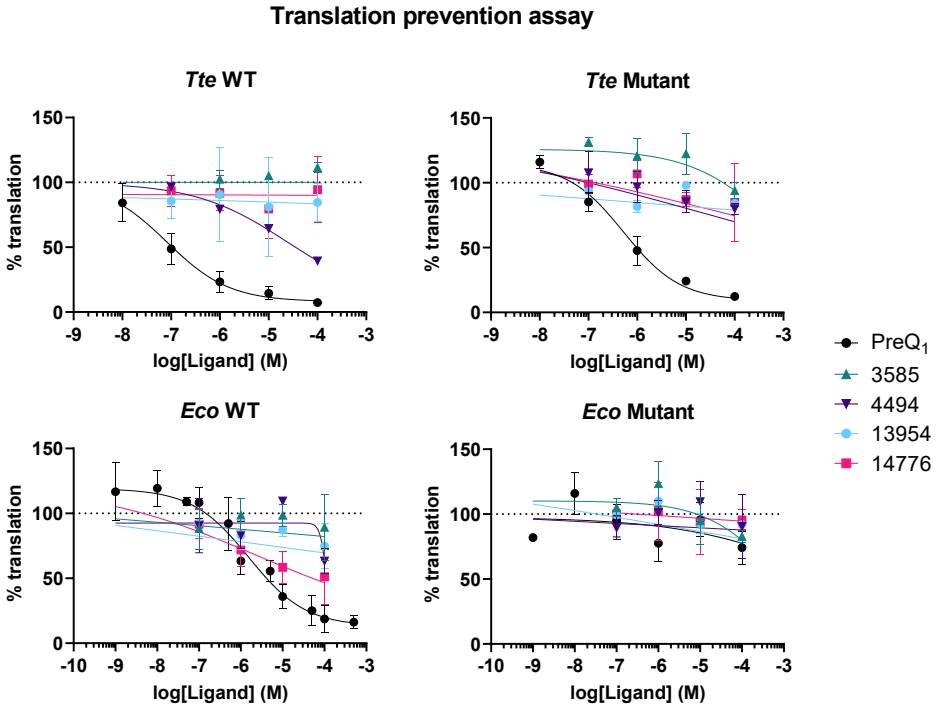

Figure 3.7. Translation prevention assays of $PreQ_1$ and hit compounds with the *Thermoanaerobacter tengcongensis* (*Tte*, top) and *Escherichia coli* (*Eco*, bottom) wildtype (WT) and C-to-U mutant $PreQ_1$ riboswitches. Translation percentages were calculated by normalizing the luminescent signal to the DMSO control. Measurements were performed in duplicate.

Compound 4494 is the most promising hit

Considering the results from the CB ASsay, frameshift assay and translation prevention assay, **4494** emerged as the most promising potential $PreQ_1$ riboswitch ligand. Compound **4494** displayed clear competitive binding on native gel, stabilized the PK conformation in a FS assay, decreased gene expression through binding to the riboswitch, and lost activity in both CB and functional assays upon mutation of the cytosine crucial for binding with $PreQ_1$. The latter suggests that **4494** may adopt a comparable binding pose to the $PreQ_1$ riboswitch as the native ligand $PreQ_1$. Upon examining the molecular structure of **4494**, indeed a striking similarity to the chemical scaffold of $PreQ_1$ becomes apparent, prompting further docking studies. Unfortunately, no high-resolution crystal structure of the *Fnu* riboswitch was available. Therefore, possible binding modes of the identified hits were docked using the *Bsu* (PDB ID: 3FU2) and *Tte* (PDB ID: 6VUI) $PreQ_1$-I_{II} riboswitches. The co-crystallized $PreQ_1$ (**Figure 3.8A and 3.8C**) was removed from the structures and replaced by the hit molecule, after which the suggested binding poses were manually inspected and selected (**Figure 3.8B and 3.8D, Figure S3.5 and S3.6**).

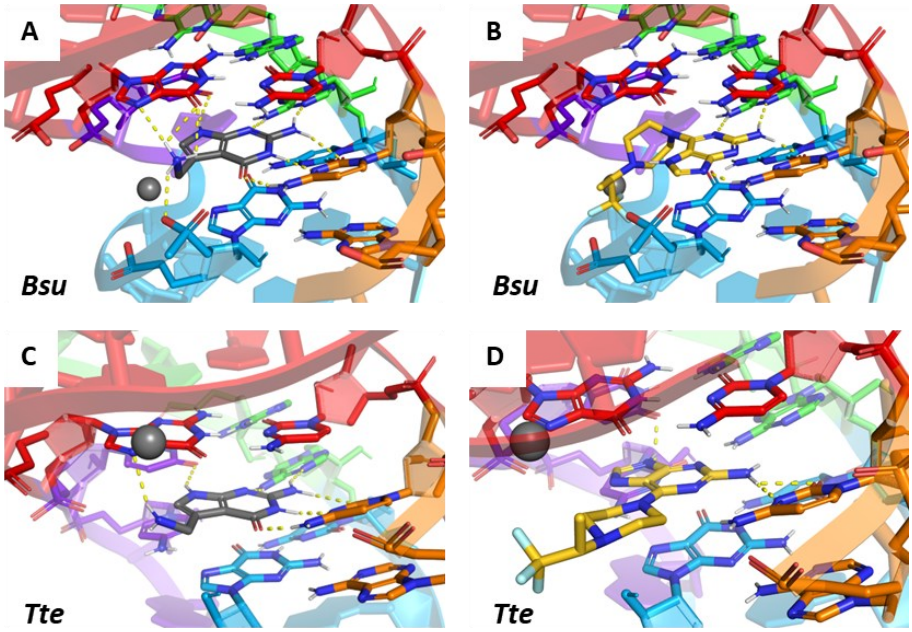

Figure 3.8. Docking of $PreQ_1$ and **4494** to the *Bacillus subtilis* (*Bsu*) (PDB ID: 3FU2) and *Thermoanaerobacter tengcongensis* (*Tte*) (PDB ID: 6VUI) $PreQ_1$-I_{II} riboswitches. Most probable binding poses of **4494** were manually selected. Hydrogen bonds are indicated with yellow dashed lines. **A)** Crystal structure of the *Bsu* $PreQ_1$ riboswitch co-crystallized with $PreQ_1$. **B)** Close-up docked structure of **4494** bound to the *Bsu* $PreQ_1$ riboswitch. **C)** Crystal structure of the *Tte* $PreQ_1$ riboswitch co-crystallized with $PreQ_1$. **D)** Close up docked structure of **4494** bound to the *Tte* $PreQ_1$ riboswitch.

The most probable docking poses of **4494** suggest that it forms hydrogen bonds with the essential cytosine, albeit at a different angle than $PreQ_1$. The $PreQ_1$ binding pocket does not allow for modifications at the carbonyl position, forcing the ligand to turn to accommodate the (2,2,2-trifluoro-1-methylethyl)-piperazine group. This is especially evident for *Bsu*, which has a narrow binding pocket that forces the ligand to turn almost 90 degrees. Alternatively, *Tte* has a larger and more accessible binding pocket, which is why it can likely accommodate docking poses that more closely resemble the $PreQ_1$ orientation. This could also explain the higher affinity of **4494** to the *Tte* riboswitch. Of note, docking indicated no preference for a specific stereoisomer. In both cases, the flipped conformation results in a mismatched hydrogen bonding scheme, potentially explaining the observed lower affinity when compared to $PreQ_1$. It must be noted that the riboswitches were modelled as rigid structures, so possible rearrangement of RNA is not taken into account in this docking analysis. In any case, the proposed docking modes offered clear opportunities for hit optimisation.

The finding that $PreQ_1$-like molecules can be modified at the WCF-face and still retain some affinity to the $PreQ_1$ riboswitch is rather surprising. Given that most published modifications to $PreQ_1$ have focused on the aminomethyl group[14,22,23,38], exploring new modifications at the carbonyl position of guanine could provide insights for developing the next generation of $PreQ_1$ riboswitch ligands. To better understand the binding pocket and the spatial constraints around the trifluoromethyl group, a small library of **4494** analogues was synthesized and evaluated in the CB ASsay and translation prevention assay (**Figure 3.9**). Specifically, small modifications were introduced to the 2,2,2-trifluoro-1-methylethyl group to assess its steric and electronic contributions. These included replacing the methyl group with a hydrogen or carbonyl (compounds **2** and **3**), or substituting the entire 2,2,2-trifluoro-1-methylethyl group by a carboxylic acid or a Boc protecting group (compounds **4** and **5**). Alternatively, partial or complete removal of the 2,2,2-trifluoro-1-methylethyl group (compounds **6** and **7**) was investigated. Substitution of the piperazine ring by a morpholine or a piperidine moiety, compounds **8** and **9** respectively, were also synthesized. Unfortunately, none of these compounds showed activity in either the CB ASsay or translation prevention assay. In fact, only starting material **1** displayed some CB activity for the *Fnu* and *Tte* riboswitch but remained inactive in the translation prevention assay. Finally, upon testing resynthesized **4494** (compound **10**), no activity was observed. This unexpected result prompted an investigation into the purity of **4494** from Enamine.

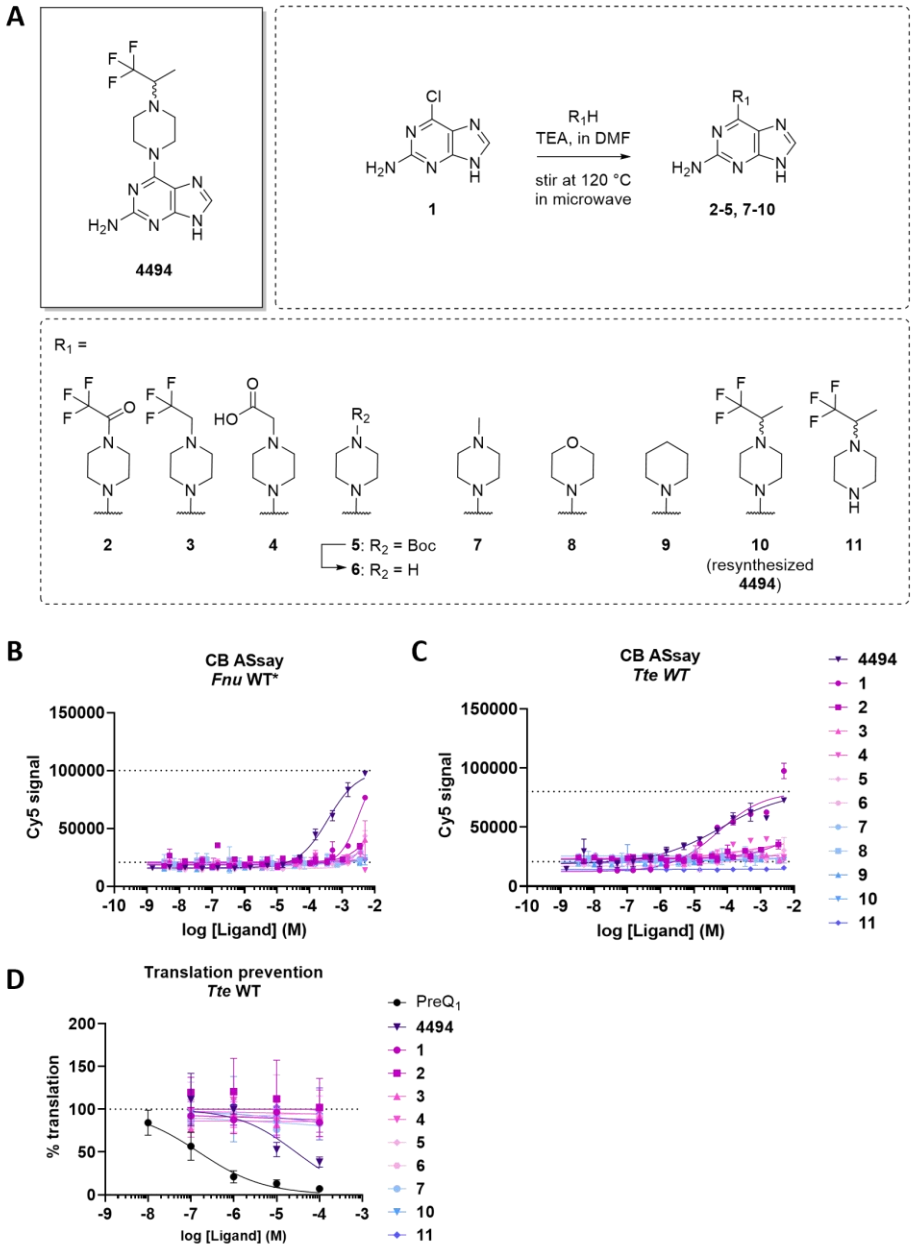

Figure 3.9. Assessment of **4494** analogues. **A)** Molecular structures and synthesis protocol of **4494** and analogues. **B-C)** Competitive binding antisense assay (CB ASsay) of identified hits for the $PreQ_1$-I riboswitches of *Fusobacterium nucleatum* (*Fnu*) wildtype* (WT*) (**B**) and *Thermoanaerobacter tengcongensis* (*Tte*) WT (**C**). Dotted lines denote the minimum and maximum Cy5 signal as determined by the positive and negative controls. **D)** Translation prevention assays of $PreQ_1$ and hit compounds with the *Thermoanaerobacter tengcongensis* (*Tte*) $PreQ_1$ riboswitch. Translation percentages were calculated by normalizing the luminescent signal to the DMSO control. Measurements were performed in duplicate.

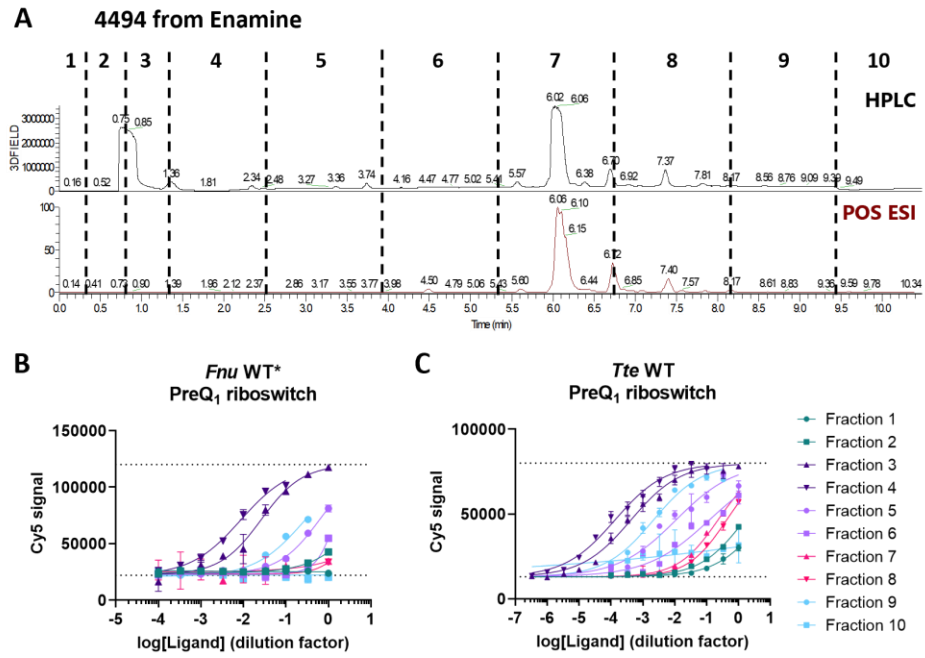

Figure 3.10. Analysis of **4494** from Enamine. **A)** LCMS of **4494** from Enamine (H_2O+0.1% TFA to 50% ACN in H_2O+0.1% TFA), with UV-Vis trace ('HPLC') and mass spectrum ('POS ESI') ranging from m/z 100-1000. Indicated with dashed lines are the fractions collected with preparative HPLC. **B-C)** Competitive binding antisense assay (CB ASsay) of fractions of **4494** from Enamine for the wildtype* (WT*) $PreQ_1$-I riboswitches of *Fusobacterium nucleatum* (*Fnu*) (**B**) and WT *Thermoanaerobacter tengcongensis* (*Tte*) (**C**). Dotted lines denote the minimum and maximum Cy5 signal as determined by the positive and negative controls.

The active impurity in compound 4494

Analysis with both LCMS and NMR showed the resynthesized compound **10** was highly pure, whereas significant impurities were present in the Enamine sample (**Figure S3.7A and S3.7B**). To rule out the unlikely possibility of having synthesized the exact opposite isomer of **4494**, a chiral column analysis was performed (**Figure S3.7C**). Both samples contained the same ratio of isomers, from which it was concluded that none of the isomers were active and that an impurity may be responsible the observed activity. Therefore, the remaining 26 mg of the **4494** batch from Enamine was purchased and split in 10 different fractions with preparative HPLC on a C18 column (**Figure 3.10**). These fractions were freeze-dried, dissolved in DMSO and tested in the CB ASsay. Fractions 3 and fraction 4 showed the highest activity, suggesting that the active compound is more polar than the main compound present in fraction 7. Fraction 4, which exhibited the highest activity, was further separated in 10 fractions using preparative HPLC (**Figure S3.8**) and tested again in the CB ASsay, revealing that subfraction 4.4 was the most active.

This fraction was highly enriched in a compound with *m/z* = 152. However, further analysis was not possible due to the limited amount of sample available. To generate a larger amount of impurity, **4494** was resynthesized using the Enamine synthesis protocol. Notably, this synthesis was performed in DMSO with DIPEA as a base, instead of DMF and TEA. Purification by preparative HPLC and subsequent testing in the CB ASsay (**Figure S3.9**) identified fraction 1 as an active fraction, indicating that the impurity is reproducible and likely forms as side-product during the synthesis of **4494**. Interestingly, *m/z* = 152 was also clearly present in fraction 1 (**Figure S3.10A**), further suggesting that this mass corresponds to the active compound. A notable compound with a mass of 151 is guanine, one of the well-known $PreQ_1$ analogues tested in Chapter 2. Guanine, analysed by LCMS (**Figure S3.10B**) exhibited the same retention time and mass as the *m/z* = 152 peaks observed in both the original **4494** and the resynthesized **4494** using the Enamine protocol. To further confirm that guanine was the active impurity, the *m/z* = 152 peak was isolated with preparative HPLC and analysed along with guanine with high resolution mass spectrometry (HRMS) (**Figure S3.10C**). The identical exact mass (calcd. for $[C_5H_6N_5O]^+$ 152.05669; found 152.05685) and peak pattern confirmed that the active impurity is guanine. Interestingly, the activity of **4494** in all assays is consistently 100-fold lower than that of guanine, suggesting that approximately 1% of the sample consists of guanine impurity (**Figure S3.11**).

It was hypothesized that guanine could have formed from the starting material, 2-amino-6-chloropurine (2a6cp) (**Figure S3.12A**). To investigate which conditions can lead to guanine formation, 2a6cp was subjected to different conditions. Heating 2a6cp to 130 °C with DIPEA in DMSO (**Figure S3.12B**), similar to the Enamine synthesis protocol, did not yield a high amount of guanine, making it unlikely that guanine is formed during the reaction. However, stirring 2a6cp with TFA in DMSO at room temperature resulted in a significant amount of guanine (**Figure S3.12C**). Notably, conversion of 2-amino-6-chloropurine to guanine by treatment with TFA in water is a commonly used synthesis strategy[39] and it was previously reported that conversion of 2a6cp to guanine in DMSO was only successful after a workup with water[40]. Therefore, it is likely that 2a6cp is converted to guanine through an acid-catalysed reaction with water. Water can be either introduced in the reaction by using non-dry DMSO, or during or after workup. Since purification of **4494** is done by preparative HPLC, where TFA is used as a counterion, it is highly likely that this is the preferred method to generate the active impurity when starting material is not consumed.

Discussion

This Chapter describes a high-throughput screening (HTS) campaign to identify ligands for $PreQ_1$-I riboswitches. The HTS was performed using the competitive binding assay (CB ASsay) for the clinically relevant *Fusobacterium nucleatum* (*Fnu*) $PreQ_1$ riboswitch, as developed in Chapter 2. The CB ASsay was easily upscaled to a HTS format, and the potential of the assay was demonstrated by conducting a HTS that lead to the discovery of four hits. These hits underwent further evaluation using CB ASsays with the *Fnu*, *Thermoanaerobacter tengcongensis* (*Tte*), *Bacillus subtilis* (*Bsu*) and *Enterococcus faecalis* (*Efa*) $PreQ_1$-I riboswitches, frameshifting assays with *Fnu*, *Tte*, *Bsu* and *Escherichia coli* (*Eco*) riboswitches and translation prevention assays with *Tte* and *Eco* riboswitches.

The most promising hit, compound **4494**, exhibited competitive binding activity for the WT* *Fnu* and WT *Tte*, *Bsu* and *Efa* riboswitches, clearly promoted *Fnu* and *Tte* pseudoknot formation when visualized on native PAGE and both stimulated frameshifting and prevented translation with the *Tte* riboswitch. In addition, activities in the competitive binding- and functional assays were diminished upon a C17U mutation of the essential cytosine in the riboswitch binding pocket, indicating a binding mode similar to that of the natural ligand $PreQ_1$. This finding was supported by molecular docking, which suggested that **4494** can be recognized in a comparable fashion by the riboswitch as native ligand $PreQ_1$, albeit at a different angle to accommodate the (2,2,2-trifluoro-1-methylethyl)-piperazine group.

The docking studies also revealed clear opportunities for ligand optimisation that could enhance the binding potency of **4494**. However, upon testing a small library of **4494** analogues and resynthesized **4494**, no activity was observed in either CB ASsay or translation prevention assay. Thorough analysis of both **4494** from Enamine and the resynthesized **4494** using the Enamine protocol led to the identification of an active impurity with m/z = 152. This impurity was confirmed to be guanine, a well-known ligand for the $PreQ_1$ riboswitch[9]. Unfortunately, it is unlikely that guanine can function as an antibiotic, as it is very poorly soluble and can be processed by bacteria[41].

While no potential antibiotic has been found, this Chapter clearly highlights the sensitivity of the CB ASsay, as it was able to pick up a ~1% guanine impurity. This Chapter also demonstrates that the CB ASsay could easily be downscaled, decreasing material usage, and enabling a higher throughput. The assay is quick, exemplified by the fact that the entire Enamine RNA focused library of 15.520 compounds was screened within a day. All materials for the HTS can be obtained from established commercial sources at a relatively

low cost, ensuring readily available high-quality materials and reducing variability between screenings.

Unfortunately, working with RNA-binding ligands posed a challenge, as these molecules often contain aromatic rings that are required for stacking interactions with RNA nucleobases. This means that the compounds can be both very apolar and thus difficult to dissolve in an aqueous buffer and sometimes have elaborate conjugated systems that can interfere with the fluorescent signal. Many false positives were identified that displayed a high Cy5 signal due to autofluorescence or light scattering by precipitation of the ligand. Alternatively, false negatives were likely present due to quenching of the Cy5 signal. While the custom KNIME data analysis workflow successfully eliminated systemic plate effects, false positives and negatives were more randomly distributed and could not be removed from the datasets. To decrease the chance of finding false positives or false negatives, the HTS was performed in duplicate and followed up by a rigorous hit selection process that included re-testing hits, together with their most active analogues, at a range of concentrations.

After repurchasing the most promising hits, compounds were evaluated with the CB ASsay at increasing concentrations. Compounds that visibly precipitated, showed a steep increase in Cy5 signal (high Hill slope) or whose Cy5-signal exceeded the positive control were classified as false positives. All remaining hits were tested with various $PreQ_1$-I riboswitches to determine hit selectivity. However, directly comparing CB activity between different $PreQ_1$ riboswitch sequences to determine hit selectivity is not straightforward, as the stringency of the CB ASsay varies greatly for different riboswitches. This is exemplified by the *Bsu* riboswitch, for which the stringency of the CB ASsay is much higher ($PreQ_1$ K_D = 50 nM[9], EC_{50} = 2.1 µM) than the *Fnu* riboswitch ($PreQ_1$ K_D = 280 nM[42], EC_{50} = 440 nM). Thus, CB activity should not be used as a direct measure to compare hit selectivity.

Direct comparison of hit activity for different $PreQ_1$ riboswitches in functional assays is also not straightforward, as activity in these assays is highly dependent on which (part of the) RNA structure is stabilized by the ligand. It is possible that a ligand binds to the RNA target but displays no activity due to stabilization of a different part of the pseudoknot. For example, compound **4494** (~1% guanine) promoted frameshifting with both the *Tte* and *Eco* riboswitches, proving that this compound can bind to and stabilize the RNA pseudoknot conformation, especially stem P1. However, **4494** (~1% guanine) only prevented translation with the *Tte* riboswitch and not with the *Eco* riboswitch. It has been

previously observed that the *Eco* riboswitch can very accurately discriminate between $PreQ_1$ and $PreQ_0$[20], and it is hypothesized that synthetic riboswitch ligands require engaging most, if not all recognition motifs of the natural ligand to correctly stabilize stem P2 and elicit a functional response[43]. This could explain why **4494** (~1% guanine), which lacks the aminomethyl group entirely, is not able to prevent translation with the *Eco* riboswitch.

One of the key challenges in RNA targeting, as discussed in this Chapter, is that ligand binding does not equate to functional activity[9,22]. Consequently, RNA ligands can be categorized into two types: those that bind RNA and elicit a functional response, and those that bind RNA without inducing functional effect. While functional ligands are the most desirable, a lack of functional response does not preclude a ligand from being a potential drug candidate. For instance, it has been proposed that simply blocking the aptamer domain of a riboswitch may be sufficient to compromise its function[43]. Alternatively, RNA ligands can be functionalized with a second ligand promoting RNA degradation (RIBOTACs[44,45] or PINADs[46]) to achieve biological activity. With this perspective, hits that exhibited only competitive binding activity (**3585**, **13954** and **14776**) could be reassessed using techniques such as microscale thermophoresis (MST) or surface plasmon resonance (SPR) to further characterize ligand-RNA engagement and binding affinity.

Perspective on targeting the $PreQ_1$ riboswitch

This research focuses on targeting $PreQ_1$ riboswitches as possible antibiotic drug targets. These riboswitches, which are not present in eukaryotic organisms, regulate the biosynthesis and transport of $PreQ_1$, a key precursor of Queuosine (Q). Q is an essential modified nucleobase that is required for translational fidelity. Disabling the Q synthesis pathway by knocking out Q synthesizing enzymes has been shown to decrease bacterial viability and virulence in *Eco* and *Shigella flexneri*, respectively[6–8]. Therefore, it is thought that the $PreQ_1$ riboswitch is an interesting antibiotic target. How absence of Q affects bacteria depends on which proteins are misfolded, and this can vary greatly between different bacterial strains. To better understand the potential consequences of depleting Q from bacteria, an experimentally validated prediction tool found that genes with high levels of NAU codons are downregulated in the absence of Q[47]. Such genes are often involved in biofilm formation and virulence. Moreover, it was predicted that many human pathogenic bacteria express virulence factors encoded by NAU-enriched genes, suggesting that their pathogenicity would thus be affected by the absence of Q. Disabling Q synthesis or salvage thus seems to hold promise for antibiotic drug development.

Bacteria can be roughly divided into two categories: Q-sources and Q-sinks. Q-sources are bacteria that harbour the full set of *de novo* Q synthesis genes (mainly Proteobacteria), whereas Q-sinks rely on salvage of queuine, $PreQ_0$ or $PreQ_1$ from the environment through transporters such as QueT and YhhQ (mainly Actinomycetota and Bacillota)[48,49]. Some bacteria contain both the Q synthesis enzymes and transporter proteins, such as *Eco*[19]. Interestingly, the *Eco* $PreQ_1$-I_{III} riboswitch regulates the expression of the YhhQ transporter, but it is not clear whether the Q synthesis enzymes are also under riboswitch control. To avoid developing drugs that will not actually deplete bacteria from Q, it would be best to target $PreQ_1$ riboswitches from bacterial strains that have either Q synthesis enzymes or Q transport proteins, but not both.

Most efforts towards finding new ligands for the $PreQ_1$ riboswitch have been directed at $PreQ_1$-I riboswitches, which is the most promising class as an antibiotic target. $PreQ_1$-I riboswitches are the smallest class of riboswitches and have a compact aptamer domain. Because of this, potential escape mutations will likely disrupt $PreQ_1$ binding or gene regulation[50]. This leaves little room for the bacterium to develop mutational resistance against new ligands, especially if the new ligand targets the native $PreQ_1$ binding pocket. On top of this, the high prevalence of $PreQ_1$-I riboswitches in different clinically relevant pathogenic strains and absence in commensal bacteria makes them especially suitable as antibiotic targets[21,51]. Similarly, $PreQ_1$-II riboswitch *in vivo* function was also greatly affected by mutations, even if $PreQ_1$ binding was rescued by compensatory mutations[43], making it less likely that these riboswitches will develop mutational resistance against a potential ligand. However, $PreQ_1$-II riboswitches are less prevalent than $PreQ_1$-I riboswitches[14]. $PreQ_1$-III riboswitches are the least prevalent of all $PreQ_1$ riboswitches and are remarkably resistant against mutations, retaining most of their gene-regulatory activity through compensatory interactions that preserve the RNA fold[50]. Therefore, $PreQ_1$-III riboswitches are unsuitable for drug development.

Even among $PreQ_1$-I riboswitches, there is significant variation in sequence, mechanism and function. Consequently, a ligand that targets a $PreQ_1$-I riboswitch from one bacterial strain may not be effective against another. To develop narrow-spectrum antibiotics, future drug discovery efforts should focus on a specific $PreQ_1$-I riboswitch from a clinically relevant bacterial strain. Before pursuing this approach, it is essential to assess the impact of disabling Q synthesis or its transport to ensure that targeting the $PreQ_1$ riboswitch will completely deplete the bacteria of Q, and that Q absence produces deleterious effects in that strain. Moreover, finding ligands that bind the native $PreQ_1$ binding pocket will

increase the chance of finding a biologically active ligand and decrease the chance of mutational resistance. Of course, hits should ultimately be evaluated with bacterial assays to assess their antibiotic potential. For such assays it must be considered that targeting the $PreQ_1$ riboswitch will not always lead to a decrease in cell growth or viability, so minimal inhibitory concentration assays should ideally be complemented with e.g. infectivity assays.

Whether or not the $PreQ_1$ riboswitch proves to be a useful antibiotic target in the future, the research in this Chapter clearly demonstrates that the CB ASsay is able to detect weak but biologically active hits for clinically relevant RNA tertiary structures. Where previous competitive binding assays were limited in the number of targetable RNA structures as they relied on competition with specific (fluorescent) binders, such as the Tat peptide from the HIV-1-TAR hairpin[52–55], the CB ASsay employs an ASO that is customizable for any RNA target. To demonstrate that the CB ASsay is applicable to other complex and clinically relevant RNA targets, the method will be applied to two RNA structures from SARS-CoV-2: the frameshifting pseudoknot (Chapter 4) and a G-quadruplex GQ-3467 (Chapter 5).

Acknowledgements

Bjorn van Doodewaerd and Paul Geurink are kindly acknowledged for their support in their HTS facility, assisting with both screenings and further hit validation. Jana Hoffmann is acknowledged for characterizing the HTS hits in the translation prevention assay. Dr. Anthe Janssen is acknowledged for docking the HTS hits to the *Bsu* and *Tte* $PreQ_1$ riboswitch structures and aiding in the design of the new generation of **4494** analogues. Victor van Kuijk is acknowledged for characterizing **4494** analogues in the CB ASsay and translation prevention assay, as well as for his perseverance during the discovery that **4494** was not the active molecule. Finally, Hans van den Elst is kindly acknowledged for his extensive assistance with the purification and analysis of **4494**, which led to the identification of the active impurity.

References

(1) Nahvi, A.; Sudarsan, N.; Ebert, M. S.; Zou, X.; Brown, K. L.; Breaker, R. R. Genetic Control by a Metabolite Binding mRNA. *Chem. Biol.* **2002**, *9* (9), 1043–1049. https://doi.org/10.1016/S1074-5521(02)00224-7.

(2) Blount, K. F.; Breaker, R. R. Riboswitches as Antibacterial Drug Targets. *Nat. Biotechnol.* **2006**, *24* (12), 1558–1564. https://doi.org/10.1038/nbt1268.

(3) Breaker, R. R. Riboswitches and the RNA World. *Cold Spring Harb. Perspect. Biol.* **2012**, *4* (2), a003566. https://doi.org/10.1101/cshperspect.a003566.

(4) Vargas-Junior, V.; Caffarena, E.; Antunes, D. Riboswitches as Antimicrobial Targets. In *Structure-Based Drug Design*; Marti, M. A., Turjanski, A. G., Fernández Do Porto, D., Eds.; Springer International Publishing: Cham, 2024; pp 81–108. https://doi.org/10.1007/978-3-031-69162-1_3.

(5) Ellinger, E.; Chauvier, A.; Romero, R. A.; Liu, Y.; Ray, S.; Walter, N. G. Riboswitches as Therapeutic Targets: Promise of a New Era of Antibiotics. *Expert Opin. Ther. Targets* **2023**, *27* (6), 433–445. https://doi.org/10.1080/14728222.2023.2230363.

(6) Iwata-Reuyl, D. Biosynthesis of the 7-Deazaguanosine Hypermodified Nucleosides of Transfer RNA. *Bioorganic Chem.* **2003**, *31* (1), 24–43. https://doi.org/10.1016/S0045-2068(02)00513-8.

(7) Durand, J. M. B.; Dagberg, B.; Uhlin, B. E.; Björk, G. R. Transfer RNA Modification, Temperature and DNA Superhelicity Have a Common Target in the Regulatory Network of the Virulence of Shigella Flexneri: The Expression of the virF Gene. *Mol. Microbiol.* **2000**, *35* (4), 924–935. https://doi.org/10.1046/j.1365-2958.2000.01767.x.

(8) Noguchi, S.; Nishimura, Y.; Hirota, Y.; Nishimura, S. Isolation and Characterization of an Escherichia Coli Mutant Lacking tRNA-Guanine Transglycosylase. Function and Biosynthesis of Queuosine in tRNA. *J. Biol. Chem.* **1982**, *257* (11), 6544–6550. https://doi.org/10.1016/S0021-9258(20)65176-6.

(9) Roth, A.; Winkler, W. C.; Regulski, E. E.; Lee, B. W. K.; Lim, J.; Jona, I.; Barrick, J. E.; Ritwik, A.; Kim, J. N.; Welz, R.; Iwata-Reuyl, D.; Breaker, R. R. A Riboswitch Selective for the Queuosine Precursor preQ1 Contains an Unusually Small Aptamer Domain. *Nat. Struct. Mol. Biol.* **2007**, *14* (4), 308–317. https://doi.org/10.1038/nsmb1224.

(10) Eichhorn, C. D.; Kang, M.; Feigon, J. Structure and Function of preQ1 Riboswitches. *Biochim. Biophys. Acta BBA - Gene Regul. Mech.* **2014**, *1839* (10), 939–950. https://doi.org/10.1016/j.bbagrm.2014.04.019.

(11) McCarty, R. M.; Bandarian, V. Biosynthesis of Pyrrolopyrimidines. *Bioorganic Chem.* **2012**, *43*, 15–25. https://doi.org/10.1016/j.bioorg.2012.01.001.

(12) Meyer, M. M.; Roth, A.; Chervin, S. M.; Garcia, G. A.; Breaker, R. R. Confirmation of a Second Natural preQ1 Aptamer Class in Streptococcaceae Bacteria. *RNA* **2008**, *14* (4), 685–695. https://doi.org/10.1261/rna.937308.

(13) Barrick, J. E.; Breaker, R. R. The Distributions, Mechanisms, and Structures of Metabolite-Binding Riboswitches. *Genome Biol.* **2007**, *8* (11), R239. https://doi.org/10.1186/gb-2007-8-11-r239.

(14) McCown, P. J.; Liang, J. J.; Weinberg, Z.; Breaker, R. R. Structural, Functional, and Taxonomic Diversity of Three PreQ1 Riboswitch Classes. *Chem. Biol.* **2014**, *21* (7), 880–889. https://doi.org/10.1016/j.chembiol.2014.05.015.

(15) Schroeder, G. M.; Cavender, C. E.; Blau, M. E.; Jenkins, J. L.; Mathews, D. H.; Wedekind, J. E. A Small RNA That Cooperatively Senses Two Stacked Metabolites in One Pocket for Gene Control. *Nat. Commun.* **2022**, *13* (1), 199. https://doi.org/10.1038/s41467-021-27790-8.

(16) Kang, M.; Peterson, R.; Feigon, J. Structural Insights into Riboswitch Control of the Biosynthesis of Queuosine, a Modified Nucleotide Found in the Anticodon of tRNA. *Mol. Cell* **2009**, *33* (6), 784–790. https://doi.org/10.1016/j.molcel.2009.02.019.

(17) Klein, D. J.; Edwards, T. E.; Ferré-D'Amaré, A. R. Cocrystal Structure of a Class I preQ1 Riboswitch Reveals a Pseudoknot Recognizing an Essential Hypermodified Nucleobase. *Nat. Struct. Mol. Biol.* **2009**, *16* (3), 343–344. https://doi.org/10.1038/nsmb.1563.

(18) Jenkins, J. L.; Krucinska, J.; McCarty, R. M.; Bandarian, V.; Wedekind, J. E. Comparison of a PreQ1 Riboswitch Aptamer in Metabolite-Bound and Free States with Implications for Gene Regulation *. *J. Biol. Chem.* **2011**, *286* (28), 24626–24637. https://doi.org/10.1074/jbc.M111.230375.

(19) Zallot, R.; Yuan, Y.; De Crécy-Lagard, V. The Escherichia Coli COG1738 Member YhhQ Is Involved in 7-Cyanodeazaguanine (preQ0) Transport. *Biomolecules* **2017**, *7* (1), 12. https://doi.org/10.3390/biom7010012.

(20) Schroeder, G. M.; Kiliushik, D.; Jenkins, J. L.; Wedekind, J. E. Structure and Function Analysis of a Type III preQ1-I Riboswitch from Escherichia Coli Reveals Direct Metabolite Sensing by the Shine-Dalgarno Sequence. *J. Biol. Chem.* **2023**, *299* (10). https://doi.org/10.1016/j.jbc.2023.105208.

(21) Kiliushik, D.; Goenner, C.; Law, M.; Schroeder, G. M.; Srivastava, Y.; Jenkins, J. L.; Wedekind, J. E. Knotty Is Nice: Metabolite Binding and RNA-Mediated Gene Regulation by the preQ1 Riboswitch Family. *J. Biol. Chem.* **2024**, 107951. https://doi.org/10.1016/j.jbc.2024.107951.

(22) Neuner, E.; Frener, M.; Lusser, A.; Micura, R. Superior Cellular Activities of Azido- over Amino-Functionalized Ligands for Engineered preQ1 Riboswitches in E.Coli. *RNA Biol.* **2018**, *15* (10), 1376–1383. https://doi.org/10.1080/15476286.2018.1534526.

(23) Balaratnam, S.; Rhodes, C.; Bume, D. D.; Connelly, C.; Lai, C. C.; Kelley, J. A.; Yazdani, K.; Homan, P. J.; Incarnato, D.; Numata, T.; Schneekloth Jr, J. S. A Chemical Probe Based on the PreQ1 Metabolite Enables Transcriptome-Wide Mapping of Binding Sites. *Nat. Commun.* **2021**, *12* (1), 5856. https://doi.org/10.1038/s41467-021-25973-x.

(24) Bereiter, R.; Flemmich, L.; Nykiel, K.; Heel, S.; Geley, S.; Hanisch, M.; Eichler, C.; Breuker, K.; Lusser, A.; Micura, R. Engineering Covalent Small Molecule–RNA Complexes in Living Cells. *Nat. Chem. Biol.* **2025**, *21* (6), 843–854. https://doi.org/10.1038/s41589-024-01801-3.

(25) Flemmich, L.; Micura, R. Synthesis of Electrophile-Tethered preQ1 Analogs for Covalent Attachment to preQ1 RNA. *Beilstein J. Org. Chem.* **2025**, *21* (1), 483–489. https://doi.org/10.3762/bjoc.21.35.

(26) Kallert, E.; Fischer, T. R.; Schneider, S.; Grimm, M.; Helm, M.; Kersten, C. Protein-Based Virtual Screening Tools Applied for RNA–Ligand Docking Identify New Binders of the preQ1-Riboswitch. *J. Chem. Inf. Model.* **2022**, *62* (17), 4134–4148. https://doi.org/10.1021/acs.jcim.2c00751.

(27) Connelly, C. M.; Numata, T.; Boer, R. E.; Moon, M. H.; Sinniah, R. S.; Barchi, J. J.; Ferré-D'Amaré, A. R.; Schneekloth, J. S. Synthetic Ligands for PreQ1 Riboswitches Provide Structural and Mechanistic Insights into Targeting RNA Tertiary Structure. *Nat. Commun.* **2019**, *10* (1), 1501. https://doi.org/10.1038/s41467-019-09493-3.

(28) Parmar, S.; Bume, D. D.; Connelly, C. M.; Boer, R. E.; Prestwood, P. R.; Wang, Z.; Labuhn, H.; Sinnadurai, K.; Feri, A.; Ouellet, J.; Homan, P.; Numata, T.; Schneekloth, J. S. Mechanistic Analysis of Riboswitch Ligand Interactions Provides Insights into Pharmacological Control over Gene Expression. *Nat. Commun.* **2024**, *15* (1), 8173. https://doi.org/10.1038/s41467-024-52235-3.

(29) Almena Rodriguez, L.; Kallert, E.; Husmann, J.-Å.; Schaubruch, K.; Meisel, K. I. S.; Schwickert, M.; Hoba, S. N.; Heermann, R.; Kersten, C. Electrostatic Anchoring in RNA-Ligand Design—Dissecting the Effects of Positive Charges on Affinity, Selectivity, Binding Kinetics, and Thermodynamics. *J. Med. Chem.* **2025**, *68* (8), 8659–8678. https://doi.org/10.1021/acs.jmedchem.5c00339.

(30) *Z-Primes (PC x NC)*. KNIME Community Hub. https://hub.knime.com/mpicbg-tds/extensions/de.mpicbg.tds.knime.hcstools.feature/latest/de.mpicbg.knime.hcs.base.nodes.qc.ZPrimesNxMFactory (accessed 2024-05-29).

(31) *Normalize Plates (Z-Score)*. KNIME Community Hub. https://hub.knime.com/mpicbg-tds/extensions/de.mpicbg.tds.knime.hcstools.feature/latest/de.mpicbg.knime.hcs.base.nodes.norm.zscore.ZScoreNormalizerNodeFactory (accessed 2024-05-29).

(32) *Normalize Plates (B-Score)*. KNIME Community Hub. https://hub.knime.com/mpicbg-tds/extensions/de.mpicbg.tds.knime.hcstools.feature/latest/de.mpicbg.knime.hcs.base.nodes.norm.BScoreNormalizerFactory (accessed 2024-05-29).

(33) Malo, N.; Hanley, J. A.; Cerquozzi, S.; Pelletier, J.; Nadon, R. Statistical Practice in High-Throughput Screening Data Analysis. *Nat. Biotechnol.* **2006**, *24* (2), 167–175. https://doi.org/10.1038/nbt1186.

(34) Turek-Etienne, T. C.; Small, E. C.; Soh, S. C.; Xin, T. A.; Gaitonde, P. V.; Barrabee, E. B.; Hart, R. F.; Bryant, R. W. Evaluation of Fluorescent Compound Interference in 4 Fluorescence Polarization Assays: 2 Kinases, 1 Protease, and 1 Phosphatase. *SLAS Discov.* **2003**, *8* (2), 176–184. https://doi.org/10.1177/1087057103252304.

(35) Lipinski, C. A.; Lombardo, F.; Dominy, B. W.; Feeney, P. J. Experimental and Computational Approaches to Estimate Solubility and Permeability in Drug Discovery and Development Settings. *Adv. Drug Deliv. Rev.* **2001**, *46* (1–3), 3–26. https://doi.org/10.1016/s0169-409x(00)00129-0.

(36) Menichelli, E.; Lam, B. J.; Wang, Y.; Wang, V. S.; Shaffer, J.; Tjhung, K. F.; Bursulaya, B.; Nguyen, T. N.; Vo, T.; Alper, P. B.; McAllister, C. S.; Jones, D. H.; Spraggon, G.; Michellys, P.-Y.; Joslin, J.; Joyce, G. F.; Rogers, J. Discovery of Small Molecules That Target a Tertiary-Structured RNA. *Proc. Natl. Acad. Sci.* **2022**, *119* (48), e2213117119. https://doi.org/10.1073/pnas.2213117119.

(37) Martin, W. J.; Grandi, P.; Marcia, M. Screening Strategies for Identifying RNA- and Ribonucleoprotein-Targeted Compounds. *Trends Pharmacol. Sci.* **2021**, *42* (9), 758–771. https://doi.org/10.1016/j.tips.2021.06.001.

(38) Bessler, L.; Kaur, N.; Vogt, L.-M.; Flemmich, L.; Siebenaller, C.; Winz, M.-L.; Tuorto, F.; Micura, R.; Ehrenhofer-Murray, A. E.; Helm, M. Functional Integration of a Semi-Synthetic Azido-Queuosine Derivative into Translation and a tRNA Modification Circuit. *Nucleic Acids Res.* **2022**, *50* (18), 10785–10800. https://doi.org/10.1093/nar/gkac822.

(39) Głowacka, I. E.; Andrei, G.; Schols, D.; Snoeck, R.; Piotrowska, D. G. Phosphonylated Acyclic Guanosine Analogues with the 1,2,3-Triazole Linker. *Molecules* **2015**, *20* (10), 18789–18807. https://doi.org/10.3390/molecules201018789.

(40) Majumdar, B.; Sarma, D.; Lee, E. M.; Setterholm, N. A.; Chaput, J. C. An Improved Synthesis of Guanosine TNA Phosphoramidite for Oligonucleotide Synthesis. *Nucleosides Nucleotides Nucleic Acids 0* (0), 1–12. https://doi.org/10.1080/15257770.2024.2369688.

(41) Pavan, M. E.; Movilla, F.; Pavan, E. E.; Di Salvo, F.; López, N. I.; Pettinari, M. J. Guanine Crystal Formation by Bacteria. *BMC Biol.* **2023**, *21* (1), 66. https://doi.org/10.1186/s12915-023-01572-8.

(42) Rieder, U.; Kreutz, C.; Micura, R. Folding of a Transcriptionally Acting PreQ1 Riboswitch. *Proc. Natl. Acad. Sci.* **2010**, *107* (24), 10804–10809. https://doi.org/10.1073/pnas.0914925107.

(43) Dutta, D.; Wedekind, J. E. Nucleobase Mutants of a Bacterial preQ1-II Riboswitch That Uncouple Metabolite Sensing from Gene Regulation. *J. Biol. Chem.* **2020**, *295* (9), 2555–2567. https://doi.org/10.1074/jbc.RA119.010755.

(44) Costales, M. G.; Matsumoto, Y.; Velagapudi, S. P.; Disney, M. D. Small Molecule Targeted Recruitment of a Nuclease to RNA. *J. Am. Chem. Soc.* **2018**, *140* (22), 6741–6744. https://doi.org/10.1021/jacs.8b01233.

(45) Haniff, H. S.; Tong, Y.; Liu, X.; Chen, J. L.; Suresh, B. M.; Andrews, R. J.; Peterson, J. M.; O'Leary, C. A.; Benhamou, R. I.; Moss, W. N.; Disney, M. D. Targeting the SARS-CoV-2 RNA Genome with Small Molecule Binders and Ribonuclease Targeting Chimera (RIBOTAC) Degraders. *ACS Cent. Sci.* **2020**, *6* (10), 1713–1721. https://doi.org/10.1021/acscentsci.0c00984.

(46) Mikutis, S.; Rebelo, M.; Yankova, E.; Gu, M.; Tang, C.; Coelho, A. R.; Yang, M.; Hazemi, M. E.; Pires de Miranda, M.; Eleftheriou, M.; Robertson, M.; Vassiliou, G. S.; Adams, D. J.; Simas, J. P.; Corzana, F.; Schneekloth, J. S. Jr.; Tzelepis, K.; Bernardes, G. J. L. Proximity-Induced Nucleic Acid Degrader (PINAD) Approach to Targeted RNA Degradation Using Small Molecules. *ACS Cent. Sci.* **2023**, *9* (5), 892–904. https://doi.org/10.1021/acscentsci.3c00015.

(47) Díaz-Rullo, J.; González-Pastor, J. E. tRNA Queuosine Modification Is Involved in Biofilm Formation and Virulence in Bacteria. *Nucleic Acids Res.* **2023**, *51* (18), 9821–9837. https://doi.org/10.1093/nar/gkad667.

(48) Quaiyum, S.; Yuan, Y.; Kuipers, P. J.; Martinelli, M.; Jaroch, M.; de Crécy-Lagard, V. Deciphering the Diversity in Bacterial Transporters That Salvage Queuosine Precursors. *Epigenomes* **2024**, *8* (2), 16. https://doi.org/10.3390/epigenomes8020016.

(49) Badilla Lobo, A.; Soutourina, O.; Peltier, J. The Current Riboswitch Landscape in Clostridioides Difficile. *Microbiology* **2024**, *170* (10), 001508. https://doi.org/10.1099/mic.0.001508.

(50) Srivastava, Y.; Akinyemi, O.; Rohe, T. C.; Pritchett, E. M.; Baker, C. D.; Sharma, A.; Jenkins, J. L.; Mathews, D. H.; Wedekind, J. E. Two Riboswitch Classes That Share a Common Ligand-Binding Fold Show Major Differences in the Ability to Accommodate Mutations. *Nucleic Acids Res.* **2024**, gkae886. https://doi.org/10.1093/nar/gkae886.

(51) Pavlova, N.; Penchovsky, R. Bioinformatics and Genomic Analyses of the Suitability of Eight Riboswitches for Antibacterial Drug Targets. *Antibiotics* **2022**, *11* (9), 1177. https://doi.org/10.3390/antibiotics11091177.

(52) Mei, H.-Y.; Mack, D. P.; Galan, A. A.; Halim, N. S.; Heldsinger, A.; Loo, J. A.; Moreland, D. W.; Sannes-Lowery, K. A.; Sharmeen, L.; Truong, H. N.; Czarnik, A. W. Discovery of Selective, Small-Molecule Inhibitors of RNA Complexes—1. The Tat Protein/TAR RNA Complexes Required for HIV-1 Transcription. *Bioorg. Med. Chem.* **1997**, *5* (6), 1173–1184. https://doi.org/10.1016/S0968-0896(97)00064-3.

(53) Gelus, N.; Bailly, C.; Hamy, F.; Klimkait, T.; Wilson, W. D.; Boykin, D. W. Inhibition of HIV-1 Tat-TAR Interaction by Diphenylfuran Derivatives: Effects of the Terminal Basic Side Chains. *Bioorg. Med. Chem.* **1999**, *7* (6), 1089–1096. https://doi.org/10.1016/S0968-0896(99)00041-3.

(54) Patwardhan, N. N.; Cai, Z.; Newson, C. N.; Hargrove, A. E. Fluorescent Peptide Displacement as a General Assay for Screening Small Molecule Libraries against RNA. *Org. Biomol. Chem.* **2019**, *17* (7), 1778–1786. https://doi.org/10.1039/C8OB02467G.

(55) Ganser, L. R.; Lee, J.; Rangadurai, A.; Merriman, D. K.; Kelly, M. L.; Kansal, A. D.; Sathyamoorthy, B.; Al-Hashimi, H. M. High-Performance Virtual Screening by Targeting a High-Resolution RNA Dynamic Ensemble. *Nat. Struct. Mol. Biol.* **2018**, *25* (5), 425–434. https://doi.org/10.1038/s41594-018-0062-4.

Materials & Methods

Materials. All labelled oligonucleotides (**Table S3.1**) were ordered from Sigma-Aldrich or IDT and were HPLC purified. All unlabelled oligonucleotides (**Table S3.1-S3.3**) were ordered from Sigma-Aldrich in desalted format and were used without further purification. All used materials were certified DNAse and RNAse free.

Competitive binding antisense assay (CB ASsay). Described in Chapter 2.

CB ASsay on native gel electrophoresis. Described in Chapter 2.

High-throughput screening with CB ASsay. The commercially available Enamine RNA-focused library, containing 15,520 compounds (10 mM in DMSO) divided over 49 384-wells Low Dead Volume (LDV) ECHO plates (Labcyte), was screened in duplicate at a final ligand concentration of 25 µM. In a typical HTS CB ASsay, 25 nL of ligand (10 mM) was added to a black 384-wells plate (Greiner Bio-One, Small Volume, 784076) using an ECHO550 Acoustic Liquid Handler (Labcyte). To this, a mixture of 0.5 µL of Cy5-PK (1 µM) and 6.5 µL CB buffer was added with a BioTek Multiflo FX dispenser (BioTek). Then, the plate was shaken for 10 s at medium speed and incubated at 22 °C for 1 h. After this, a mixture of 0.5 µL of IBRQ-ASO (1 µM) and 2.5 µL CB buffer was added with the Multiflo dispenser, after which the plate was shaken for 10 s at medium speed, centrifuged for 1 min at 111 RCF and subsequently incubated at 22 °C for 2.5 h. The fluorescence was measured with a CLARIOstar (BMG LABTECH) using λ_{ex} = 610 ± 30 nm, λ_{em} = 675 ± 50 nm, gain = 2200 and focal point = 10.2.

Raw fluorescence data were analysed in KNIME Analytics Platform with a custom workflow (see Supporting KNIME files). For all plates, Z'-scores were calculated to confirm high quality screening data[30]. Data were normalized with standard KNIME nodes to yield Z-scores and B-scores[31,32]. Hits were determined based on calculated B-scores, differentiating between two hit categories: 'High activity hit' (B-score >10) in a single screening, and 'Moderate activity hit' (B-score 5 – 10) in both screenings. Additionally, compounds with a B-score 3 - 10 in both screenings were manually inspected to prevent premature exclusion of potential hits. Initial hits were then manually grouped based on molecular structure, and close analogues with a SUM B-score of >6 (from both screenings) were included in subsequent hit confirmation.

Computational modelling of hits. Molecular docking was performed using the ICM Molsoft Pro suite. Briefly, the structure of the *Bsu* $PreQ_1$ riboswitch in complex with $PreQ_1$ (7-deaza-7-aminomethyl-guanine) (PDB ID: 3FU2) or *Tte* riboswitch (PDB: 6VUI) was

retrieved from the Protein Data Bank using ICM Molsoft's inbuilt feature. Of this structure chain C (3FU2) or chain A (6VUI) was converted to an ICM object, with 'optimise hydrogens' set to true. 'Tight' water molecules were retained, however this led to no conserved water molecules being present. The bound ligand was isolated to a separate object. The 3D pocket finding tool was utilized to identify the binding site. Of the potential binding sites identified, the pocket containing the co-crystallized ligand was selected. A docking project was set up based on this selection using default settings. The identified hits and their relevant tautomeric forms were loaded from an SD-file and docked with the 'thoroughness' parameter set to 10, and the 10 best poses were retained. The resulting poses were manually inspected, selected, and visualized using the Open Source PyMOL application.

Translation prevention assay. Described in Chapter 2.

Frameshift assay. Described in Chapter 2.

General synthesis experimental details. All reagents were of commercial grade and were used as received unless stated otherwise. *N*,*N*-dimethylformamide (DMF) was stored over 4 Å molecular sieves that were dried *in vacuo* before use. All reactions were performed under an argon atmosphere unless stated otherwise. Solvents used for column chromatography were of pro analysis quality. Microwave syntheses were performed with the Biotage® Initiator+ microwave system using the 0.5-2.0 mL microwave vial types sealed with microwave caps (Screening devices, product# 130-3531) under the 'normal' absorption level setting. Reactions were monitored by analytical thin-layer chromatography (TLC) using Merck aluminium sheets pre-coated with silica gel 60 with detection by UV absorption (254 nm) and by spraying with a solution of ninhydrin followed by charring at ~150 °C. Column chromatography was performed manually using Screening Device silica gel 60 (0.04 - 0.063 mm) in the indicated solvents. ^{1}H NMR and ^{13}C NMR spectra were recorded on a Bruker AV-400 (400/100 MHz) spectrometer in the given solvent. Chemical shifts are given in ppm relative to the DMSO residual solvent peak. Coupling constants are given in Hz. All given ^{13}C spectra are proton decoupled. The following abbreviations are used to describe peak patterns when appropriate: s (singlet), d (doublet), dd (double doublet), t (triplet), q (quintet), m (multiplet). 2D NMR experiments (HSQC and COSY) were carried out to assign protons and carbons of the new structures and assignment follows the general numbering shown in **Figure 3.11**. Liquid chromatography-mass spectrometry (LCMS) analysis was performed on an LCQ Advantage Max (Thermo Finnigan) ion-trap spectrometer (ESI^+) coupled to a Surveyor

HPLC system (Thermo Finnigan) equipped with a C_{18} column (Gemini, 4.6 mm x 50 mm, 3 µm particle size, Phenomenex). The applied buffers were H_2O, acetonitrile (MeCN) and 1% aqueous TFA. Chiral column analysis was performed with an UltiMate 3000 UHPLC system (Thermo Scientific) equipped with a Daicel Chiracel OJ column (4.6 mm x 250 mm, 10 µm particle size). The applied eluent was 7% isopropyl alcohol in n-heptane supplemented with 0.035% diethylamine with a flow of 1 mL/min for 30 min. For reversed-phase HPLC-MS purifications, an Agilent Technologies 1260 Infinity II series prepLCMS with an Agilent Technologies InfinityLab LC/MSD XT mass spectrometer was used equipped with a VP NUCLEODUR C_{18} Gravity column (10 mm x 250 mm, 5 µm particle size) and buffers A: 0.2% TFA in H_2O and B: MeCN. A typical prep-LCMS run applied a solvent gradient from 5% to 55% B in 12 min with a flow of 5 mL/min. Collected fractions were evaporated *in vacuo*, freeze-dried and redissolved in DMSO for further analysis. High-resolution mass spectra (HRMS) were recorded with a Q-Exactive HF Orbitrap (Thermo Scientific) equipped with an electrospray ion source (ESI) (source voltage of 2.5 kV, capillary temperature 275 °C, no sheath gas, resolution = 240.000 at *m/z* = 400, mass range *m/z* = 160-2000). Injection of 2 µL of a 1 µM solution via Ultimate 3000 nano UPLC (Dionex) system with an external calibration (Thermo Scientific). The applied eluent was 50% (v/v) MeCN in H_2O supplemented with 0.1% formic acid.

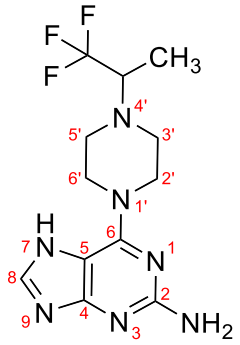

Figure 3.11. General numbering of (hetero)atoms for NMR peak assignment.

Synthesis and characterization data of compounds 2-10.

1-(4-(2-Amino-7*H*-purin-6-yl)piperazin-1-yl)-2,2,2-trifluoroethan-1-one (2).

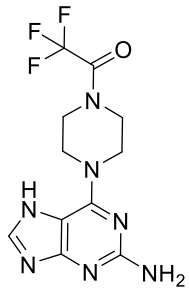

2

2-Amino-6-chloropurine (0.056 g, 0.3 mmol) was added to a mixture of 2,2,2-trifluoro-1-(piperazin-1-yl)ethan-1-one HCl (0.116 g, 0.6 mmol), triethylamine (0.17 mL, 1.2 mmol) and dry DMF (1.5 mL). The reaction mixture was stirred in the microwave at 120 °C for 60 min, cooled to room temperature and directly purified with silica gel column chromatography, using a solvent gradient from DCM:MeOH (19:1 to 9:1) to provide the title compound **2** (59.7 mg, 0.19 mmol, 63%). **^{1}H NMR** (400 MHz, DMSO-d_6): δ 12.28 (s, 1H, NH), 7.74 (s, 1H, CH-8), 5.86 (s, 2H, NH_2), 4.26 – 4.21 (m, 4H, CH-2′ and CH-6′), 3.70 (dd, J = 6.6, 4.0 Hz, 4H, CH-3′ and CH-5′). **^{13}C NMR** (101 MHz, DMSO-d_6) δ 160.1 (C-4), 154.6 (C-6), 153.8 (C-2), 135.8 (C-8), 118.3 (CF_3), 113.8 (C-5), 46.0 (C-3′ and C-5′), 43.6 (C-2′ and C-6′). **HRMS:** calcd. for $[C_{11}H_{13}F_3N_7O]^+$ 316.11282; found 316.11313.

6-(4-(2,2,2-Trifluoroethyl)piperazin-1-yl)-7*H*-purin-2-amine (3).

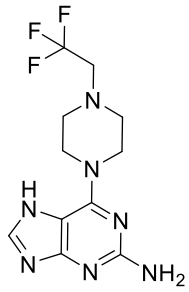

3

2-Amino-6-chloropurine (0.053 g, 0.3 mmol) was added to a mixture of 1-(2,2,2-trifluoroethyl)piperazine 2 HCl (0.155 g, 0.6 mmol), triethylamine (0.21 mL, 1.5 mmol) and dry DMF (1.5 mL). The reaction mixture was stirred in the microwave at 120 °C for 60 min. The crystalline crude was dissolved in DCM:MeOH (19:1) and concentrated *in vacuo* at 60 °C. The viscous mixture was subsequently purified with silica gel column chromatography, using a solvent gradient from DCM:MeOH (19:1 to 9:1) to provide the title compound **3** (73.7 mg, 0.25 mmol, 82%). **^{1}H NMR** (400 MHz, DMSO-d_6): δ 12.21 (s, 1H, NH), 7.69 (s, 1H, CH-8), 5.77 (s, 2H, NH_2), 4.13 (s, 4H, CH-2′ and CH-6′), 3.22 (q, J = 10.2 Hz, 2H, CH_2CF_3), 2.69 (t, J = 5.0 Hz, 4H, CH-3′ and CH-5′). **^{13}C NMR** (101 MHz, DMSO-d_6) δ 160.1 (C-4), 154.4 (C-6), 154.0 (C-2), 135.3 (C-8), 128.0 (CF_3), 113.7 (C-5), 57.7 (CH_2), 53.6 (C-3′ and C-5′), 44.8 (C-2′ and C-6′). **HRMS:** calcd. for $[C_{11}H_{15}F_3N_7]^+$ 302.13355; found 302.13363.

2-(4-(2-Amino-7*H*-purin-6-yl)piperazin-1-yl)acetic acid (4).

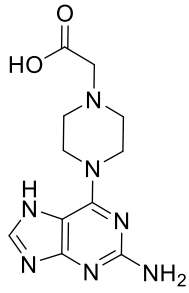

4

2-Amino-6-chloropurine (0.055 g, 0.3 mmol) was added to a mixture of 2-(piperazin-1-yl)acetic acid (0.085 g, 0.6 mmol), triethylamine (0.125 mL, 0.9 mmol) and dry DMF (1.5 mL). The reaction mixture was stirred in the microwave at 120 °C for 60 min. The crude was concentrated *in vacuo* at 60 °C and partly re-dissolved in DCM:MeOH (19:1)+NH_3OH to yield a white suspension. The filtrate was discarded, and the residue was triturated in MeOH for 48 h and filtered to remove further impurities. This yielded the title compound **4** (6.0 mg, 0.02 mmol, 7%) as an off-white powder. **^{1}H NMR** (400 MHz, DMSO-d_6): δ 12.19 (s, 1H, NH), 7.68 (s, 1H, CH-8), 5.76 (s, 2H, NH_2), 4.15 (s, 4H, CH-2′ and CH-6′), 3.19 (s, 2H, CH_2), 2.64 (t, J = 5.0 Hz, 4H, CH-3′ and CH-5′). **HRMS:** calcd. for $[C_{11}H_{16}N_7O_2]^+$ 278.13600; found 278.13615.

***Tert*-butyl 4-(2-amino-7*H*-purin-6-yl)piperazine-1-carboxylate (5).**

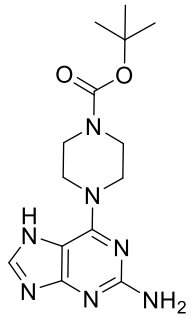

5

2-Amino-6-chloropurine (0.057 mg, 0.3 mmol) was added to a mixture of 1-Boc-piperazine (0.136 mg, 0.6 mmol), triethylamine (0.125 mL, 0.9 mmol) and dry DMF (2 mL). The reaction mixture was stirred at 80 °C for 24 h to yield an orange solution, which was quenched with milli-Q water and extracted with EtOAc and diethylether. The organic layer was washed with brine, dried with $MgSO_4$ and evaporated under reduced pressure. Purification with silica gel column chromatography, using a solvent gradient from $CHCl_3$ to $CHCl_3$:MeOH (9:1), provided the title compound **5** (30.0 mg, 0.09 mmol, 31%). **^{1}H NMR** (400 MHz, DMSO-d_6): δ 12.23 (s, 1H, NH), 7.71 (s, 1H, CH-8), 5.80 (s, 2H, NH_2), 4.11 (s, 4H, CH-2′ and CH-6′), 3.41 (dd, J = 6.3, 3.8 Hz, 4H, CH-3′ and CH-5′), 1.43 (s, 9H, $C(CH_3)_3$). **^{13}C NMR** (101 MHz, DMSO-d_6) δ 160.1 (C-4), 154.5 (C-6), 154.0 (C-2), 135.5 (C-8), 113.7 (C-5), 79.6 ($C(CH_3)_3$), 43.9 (C-2′, C-3′, C-5′ and C-6′), 28.5 ($C(CH_3)_3$). **HRMS:** calcd. for $[C_{14}H_{22}N_7O_2]^+$ 320.18295; found 320.18296.

6-(Piperazin-1-yl)-7*H*-purin-2-amine (6).

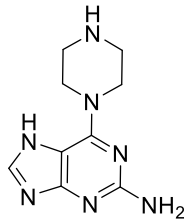

6

Compound **5** (0.070 mg, 0.3 mmol) was dissolved in dioxane (2.5 mL), to which a solution of 4M HCl in dioxane was slowly added. After 50 min, the reaction was evaporated *in vacuo*, re-dissolved in DCM:MeOH (9:1) and aqueous ammonia (few drops) and purified with silica gel column chromatography, using a solvent gradient from DCM:MeOH (19:1 to 9:1) supplemented with aqueous ammonia to provide the title compound **6** (35.5 mg, 0.16 mmol, 74%). **^{1}H NMR** (400 MHz, DMSO-d_6): δ 12.15 (s, 1H, NH), 7.67 (s, 1H, CH-8), 5.73 (s, 2H, NH_2), 4.09 (s, 4H, CH-2′ and CH-6′), 2.82 (t, J = 5.1 Hz, 4H, CH-3′ and CH-5′). **HRMS:** calcd. for $[C_9H_{14}N_7]^+$ 220.13052; found 220.13077.

6-(4-Methylpiperazin-1-yl)-7*H*-purin-2-amine (7).

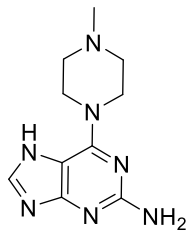

7

2-Amino-6-chloropurine (0.056 mg, 0.3 mmol) was added to a mixture of 1-methyl-piperazine (0.060 mg, 0.6 mmol), triethylamine (0.125 mL, 0.9 mmol) and dry DMF (1.5 mL), and stirred in the microwave at 120 °C for 60 min. The crude was concentrated *in vacuo* at 60 °C, re-dissolved in DCM:MeOH (9:1) and aqueous ammonia (few drops) and filtered over a glass filter to remove the precipitate. The filtrate was subsequently purified with silica gel column chromatography, using a solvent gradient from DCM:MeOH (19:1 to 9:1) supplemented with aqueous ammonia, to provide the title compound **7** (33.4 mg, 0.14 mmol, 47%). **^{1}H NMR** (400 MHz, DMSO-d_6): δ 12.19 (s, 1H, NH), 7.68 (s, 1H, CH-8), 5.75 (s, 2H, NH_2), 4.12 (s, 4H, CH-2′ and CH-6′), 2.38 (t, J = 5.0 Hz, 4H, CH-3′ and CH-5′), 2.21 (s, 3H, CH_3). **^{13}C NMR** (101 MHz, DMSO-d_6) δ 160.1 (C-4), 154.4 (C-6), 154.1 (C-2), 135.4 (C-8), 113.7 (C-5), 55.2 (C-3′ and C-5′), 46.4 (CH_3), 44.7 (C-2′ and C-6′). **HRMS:** calcd. for $[C_{10}H_{16}N_7]^+$ 234.14617; found 234.14635.

6-Morpholino-7*H*-purin-2-amine (8).

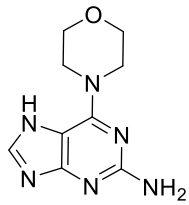

8

2-Amino-6-chloropurine (0.052 mg, 0.3 mmol) was added to a mixture of morpholine (0.052 mg, 0.6 mmol), triethylamine (0.125 mL, 0.9 mmol) and dry DMF (2 mL). The reaction mixture was stirred at 85 °C for 18 h to yield a yellow/orange solution, which was quenched with milli-Q water and extracted with EtOAc. The organic layer was dry-loaded on a silica gel column and purified with column chromatography, using a solvent gradient with DCM:MeOH (19:1 to 9:1), provided the title compound **8** (42.2 mg, 0.19 mmol, 64%). **^{1}H NMR** (400 MHz, DMSO-d_6): δ 12.22 (s, 1H, NH), 7.69 (s, 1H, CH-8), 5.79 (s, 2H, NH_2), 4.11 (s, 4H, CH-2′ and CH-6′), 3.68 (dd, J = 5.5, 4.1 Hz, 4H, CH-3′ and CH-5′). **^{13}C NMR** (101 MHz, DMSO-d_6) δ 160.1 (C-4), 154.5 (C-6), 154.1 (C-2), 134.9 (C-8), 113.8 (C-5), 66.8 (C-3′ and C-5′), 45.5 (C-2′ and C-6′). **HRMS:** calcd. for $[C_{10}H_{13}N_6O]^+$ 221.11454; found 221.11471.

6-(Piperidin-1-yl)-7*H*-purin-2-amine (9).

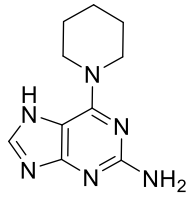

9

2-Amino-6-chloropurine (0.052 mg, 0.3 mmol) was added to a mixture of piperidine (0.051 mg, 0.6 mmol), triethylamine (0.125 mL, 0.9 mmol) and dry DMF (2 mL). The reaction mixture was stirred at 85 °C for 19 h to yield a dark orange/brown solution, which was quenched with milli-Q water and extracted with EtOAc. The organic layer was loaded on a silica gel column and purified with column chromatography, using a solvent gradient with DCM:MeOH (19:1 to 9:1), provided the title compound **9** (34.9 mg, 0.16 mmol, 54%). **^{1}H NMR** (400 MHz, DMSO-d_6): δ 12.15 (s, 1H, NH), 7.66 (s, 1H, CH-8), 5.69 (s, 2H, NH_2), 4.10 (s, 4H, CH-2′ and CH-6′), 1.70 – 1.59 (m, 2H, CH-4′)), 1.53 (td, J = 6.8, 4.2 Hz, 4H, CH-3′ and CH-5′). **^{13}C NMR** (101 MHz, DMSO-d_6) δ 160.1 (C-4), 154.3 (C-6), 154.0 (C-2), 134.9 (C-8), 113.6 (C-5), 45.8 (C-2′ and C-6′), 26.3 (C-3′ and C-5′), 25.0 (C-4′). **HRMS:** calcd. for $[C_{10}H_{15}N_6]^+$ 219.13527; found 219.13534.

6-(4-(1,1,1-Trifluoropropan-2-yl)piperazin-1-yl)-7*H*-purin-2-amine (10).

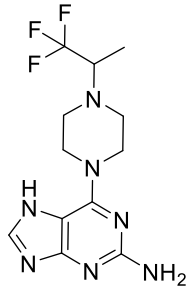

10

2-Amino-6-chloropurine (0.030 mg, 0.15 mmol) was added to a mixture of 1-(1,1,1-trifluoropropan-2-yl)piperazine (0.054 mg, 0.3 mmol), triethylamine (0.063 mL, 0.45 mmol) and dry DMF (1 mL). The reaction mixture was stirred in the microwave at 120 °C for 60 min, concentrated *in vacuo* and directly purified with silica gel column chromatography, using a solvent gradient from DCM:MeOH (19:1 to 9:1) and aqueous ammonia (few drops). The remaining impurities were removed using column chromatography with a solvent gradient from DCM:MeOH (19:1 to 9:1) without aqueous ammonia, to provide the title compound **10** (49.5 mg, 0.16 mmol, 88%). **^{1}H NMR** (400 MHz, DMSO-d_6): δ 12.20 (s, 1H, NH), 7.68 (s, 1H, CH-8), 5.76 (s, 2H, NH_2), 4.12 (s, 4H, CH-2′ and CH-6′), 2.79 – 2.63 (m, 4H, CH-3′ and CH-5′), 1.18 (d, J = 7.0 Hz, 3H, CHCH_3), 1.11 (s, 1H, CHCH$_3$). **^{13}C NMR** (101 MHz, DMSO-d_6) δ 160.1 (C-4), 154.4 (C-6), 154.0 (C-2), 135.4 (C-8), 129.2 (CF_3), 113.7 (C-5), 56.0 (CHCH$_3$), 49.5 (C-2′, C-3′, C-5′ and C-6′), 9.7 (CHCH_3). **HRMS:** calcd. for $[C_{12}H_{17}F_3N_7]^+$ 316.14920; found 316.14933.

Supplementary Information

Table S3.1. Sequences of the **competitive binding antisense assay (CB ASsay)**. RNA indicated in black. Linker (DNA) indicated in red. DNA indicated in blue. Mutated bases are underlined.

Name	Sequence (5′ → 3′)
Cy5-PrQ-FnuWT*	AGAUGUUCUAGCAAAACCAUCUUUAAAAAACUAGACCCTT[Cy5]
Cy5-PrQ-FnuMut	AGAUGUUCUAGCAAAAUCAUCUUUAAAAAACUAGACCCTT[Cy5]
IRBQ-ANTI-PrQFnu	[IBRQ]TGGTCTAGTTTTT
ANTI-Fnu-GT	TGGTCTAGTTTTT
Cy5-PrQ-Tte	CUGGGUCGCAGUAACCCCAGUUAACAAAACAAGCCTT[Cy5]
IBRQ-ANTI-PrQTte	[IBRQ]TGGCTTGTTTTAT
ANTI-Tte-GGT-3	TGGCTTGTTTTAT
Cy5-PrQ-Bsu	AGAGGUUCUAGCUACACCCUCUAUAAAAAACUAACCTT[Cy5]
IBRQ-ANTI-PrQBsu	[IBRQ]TGGTTAGTTTTTTA
ANTI-Bsu-GGT-1	TGGTTAGTTTTTTA
Cy5-PrQ-Efa	ACUGGUUCGGAAACUUCCCAGAAUAAAAAACUAAGCCTT[Cy5]
IBRQ-ANTI-PrQEfa	[IBRQ]TGGCTTAGTTTTT
ANTI-Efa-GGT-1	TGGCTTAGTTTTT
COV-PKdL3- Cy5	GGUGUAAGUGCAGCCCGUCUUACACCAUAAAUACAGGGCUCCTT[Cy5]
IBRQ-ANTI-PKdL3-TGG4	[IBRQ]TGGAGCCCUGUAUUUAU
ANTI-PKdL3-TGG-4	TGGAGCCCUGUAUUUAU
GQ3467-IBRQ	CAUGGAGGAGGUGUUGCAGGAGCCTT[IBRQ]
Cy5-ANTI-TGG-6	[Cy5]TGGCTCCTGCAA
ANTI-GQ3467-TGG-6	TGGCTCCTGCAA

Table S3.2. Sequences of the **Translation prevention assay**. The T7 polymerase promotor is indicated in green. $PreQ_1$ riboswitch sequences indicated in orange. The essential cytosine (wildtype, WT) or thymine (mutant) are underlined.

Name	Sequence (5′ → 3′)
Tte-WT fwd	TTAATACGACTCACTATAGGAATAACTGGGTCGCAGTAACCCCAGTAAAAAAAC AAGGTACAATATGGTTTCAGGATGGC
Tte-Mutant fwd	TTAATACGACTCACTATAGGAATAACTGGGTCGCAGTAATCCCAGTAAAAAAAC AAGGTACAATATGGTTTCAGGATGGC
Tte-rev	ATCAGCTAATTTTTTTAAATAAGCGCCATCCTGAAACCAT
Eco-WT fwd	TTAATACGACTCACTATAGGAATAATTGGGTTCCCTCACCCCAATCATAAAAAG GTACAATATGGTTTCAGGATGGC
Eco-Mutant fwd	TTAATACGACTCACTATAGGAATAATTGGGTTCCCTCATCCCAATCATAAAAAG GTACAATATGGTTTCAGGATGGC
Eco-rev	ATCAGCTAATTTTTTTAAATAAGCGCCATCCTGAAACCAT

Table S3.3. Sequences of the **Frameshifting assay**. $PreQ_1$ riboswitch sequences indicated in orange.

Name	**Sequence (5′ → 3′)**
T7sm-g	GGTAATACGACTCACTATAGGGAATTCTAGAAAGGAGATACCACCATG
pucrev3	CACGTTGTAAAACGACGGCCAGT
FS *Fnu* insert	CTAGTGACGCGGTGCTGGCAAAACCCGCGTAAAAAAACCAG
FS *Bsu* insert	CTAGTGCGCGGTTCTAGCTACACCCGCGTAAAAAAACTAAG
FS *Tte* insert	CTAGTGCGCGGTCGCAGTAACCCGCGTAAAAAAACAAG
FS *Eco* insert	CTAGTGCGCGGTTCCCTCACCCGCGTAAAAAAAAGGTT

Sequence entire PCR product with *Fnu* insert (5′ → 3′)

GGTAATACGACTCACTATAGGGAATTCTAGAAAGGAGATACCACCATGGCAGTGACCGGCTACCGG
CTGTTCGAGGAGATTCTGGCGGCCGCTGGTGGCGGGAGCGGAGGTGGAGGGTCGTCAGGTACCTTT
TTAAACTAGTGACGCGGTGCTGGCAAAACCCGCGTAAAAAAACCAGACAGCTTATCGCCATGGTCT
TCACACTCGAAGATTTCGTTGGGGACTGGGAACAGACAGCCGCCTACAACCTGGACCAAGTCCTTG
AACAGGGAGGTGTGTCCAGTTTGCTGCAGAATCTCGCCGTGTCCGTAACTCCGATCCAAAGGATTG
TCCGGAGCGGTGAAAATGCCCTGAAGATCGACATCCATGTCATCATCCCGTATGAAGGTCTGAGCG
CCGACCAAATGGCCCAGATCGAAGAGGTGTTTAAGGTGGTGTACCCTGTGGATGATCATCACTTTA
AGGTGATCCTGCCCTATGGCACACTGGTAATCGACGGGGTTACGCCGAACATGCTGAACTATTTCG
GACGGCCGTATGAAGGCATCGCCGTGTTCGACGGCAAAAAGATCACTGTAACAGGGACCCTGTGGA
ACGGCAACAAAATTATCGACGAGCGCCTGATCACCCCCGACGGCTCCATGCTGTTCCGAGTAACCA
TCAACAGCAGATCTAGCGGTGGTGGCGGGAGCGGCGGTGGAGGGTCATCGGGTTGTACAGAGATTG
CAGCGCTGGAGAAGGAGATCGCTGCGCTGGAGAAGGAGATTGCAGCGTTGGAGAAGGAGATCGCGG
CACTGGAGAAGGGCTAGCGGGCCCGAGTACCGAGCTCGAATTCACTGGCCGTCGTTTTACAACGTG

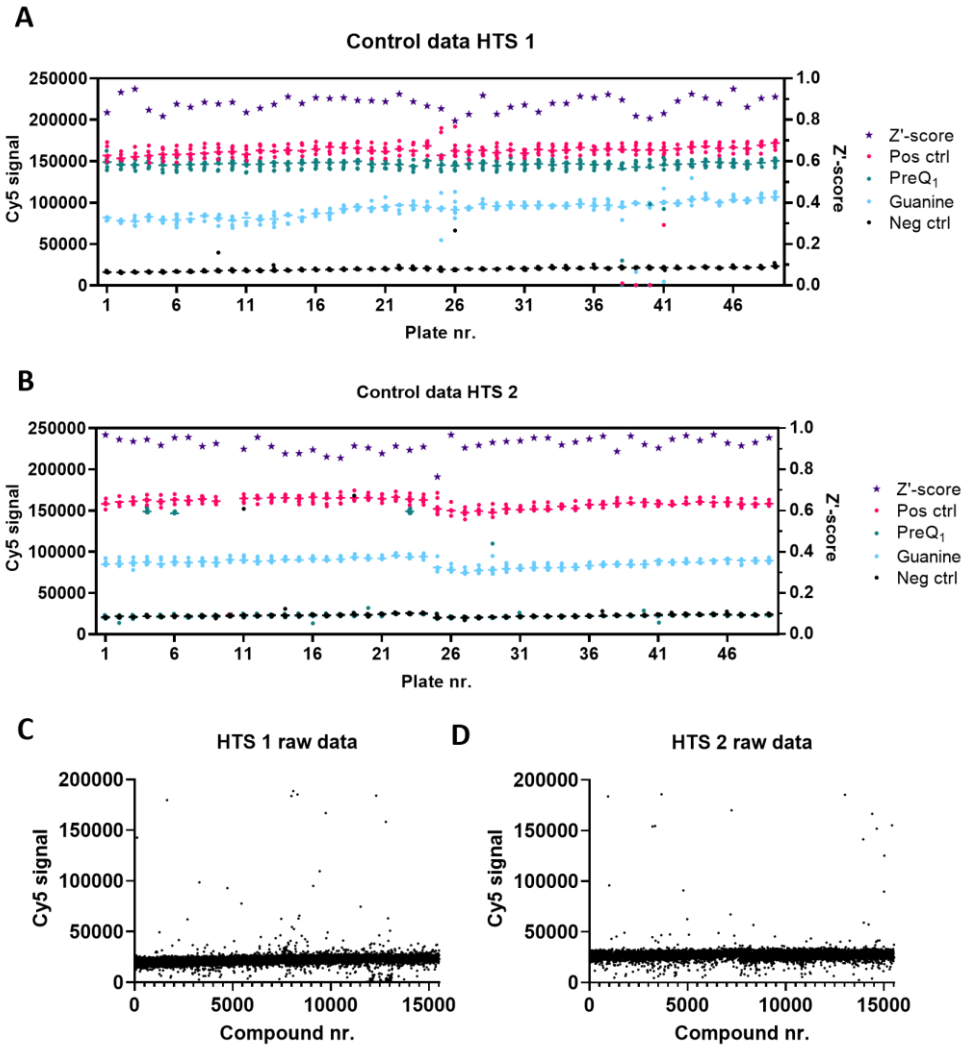

Figure S3.1. High-throughput screening (HTS) of the *Fusobacterium nucleatum* (*Fnu*) $PreQ_1$-I riboswitch with the Enamine RNA-focused library: controls and raw data. **A-B)** Controls for HTS 1 (**A**) and HTS 2 (**B**), including on the left Y-axis the Cy5-signal of the positive control (10 eq. unlabelled antisense oligonucleotide), negative control (DMSO), $PreQ_1$ (25 µM) and guanine (25 µM), and on the right Y-axis the calculated Z'-scores. **C-D)** Raw fluorescence data of HTS 1 (**C**) and HTS 2 (**D**).

Table S3.4. Summary of high-throughput screening (HTS) and hit validation data of promising hits for the *Fusobacterium nucleatum* (*Fnu*) $PreQ_1$ riboswitch. All data was normalized to the DMSO control for ease of comparison, and a colour gradient indicates low (green) to high (red) values. HTS data from both screenings, hit confirmation 1 (100 µM) and hit confirmation 2 (5, 25, 50 and 100 µM) are shown. Compounds highlighted in blue were selected for re-purchase ('most promising hits').

Hit	Data normalized to DMSO ctrl (% Cy5 signal)													
	HTS (25 µM)		Hit confirmation (100 µM)				CB_{50} measurement (µM)							
	HTS 1	HTS 2	1	2	3	4	0	5	5	25	25	50	50	100
1116	168	175	117	119	126	126	102	97	98	99	95	123	128	115
3506	97	130	98	144			102	104	102	557	99	101	100	98
3535	151	131	166	165			100	92	97	93	93	147	146	187
3585	170	110	164	163	181	165	100	102	99	100	102	108	106	180
3944	130	125	113	108			101	103	101	103	101	113	143	126
4316	141	122	126	104			97	101	99	84	99	99	104	116
4494	136	149	214	218	237	240	97	110	107	495	139	191	176	236
5065	191	182	139	149	159	111	101	97	99	94	89	93	93	290
7186	199	245	385	369			101	108	113	140	494	206	223	543
7239	82	621	133	182	189	147	100	100	97	96	99	94	89	205
7245	126	121	164	176	172	168	100	97	103	97	98	136	112	169
7426	202	137	110	186	201	175	100	96	97	96	97	101	97	244
11048	108	163	158	161	105	107	100	100	97	94	79	161	147	179
11229	104	135	257	268			99	96	96	93	96	106	121	254
12076	168	151	281	108			103	97	100	94	98	95	99	236
12576	132	131	125	128			104	109	109	111	114	114	119	124
13954	112	124	135	141			101	101	101	102	99	107	106	144
14085	155	134	104	107	121	114	98	101	99	97	98	103	102	117
14670	134	153	166	169			108	110	109	117	122	134	130	154
14776	153	156	16	26			101	116	116	182	186	213	202	73
15025	124	470	134	132			101	101	102	109	109	120	113	129

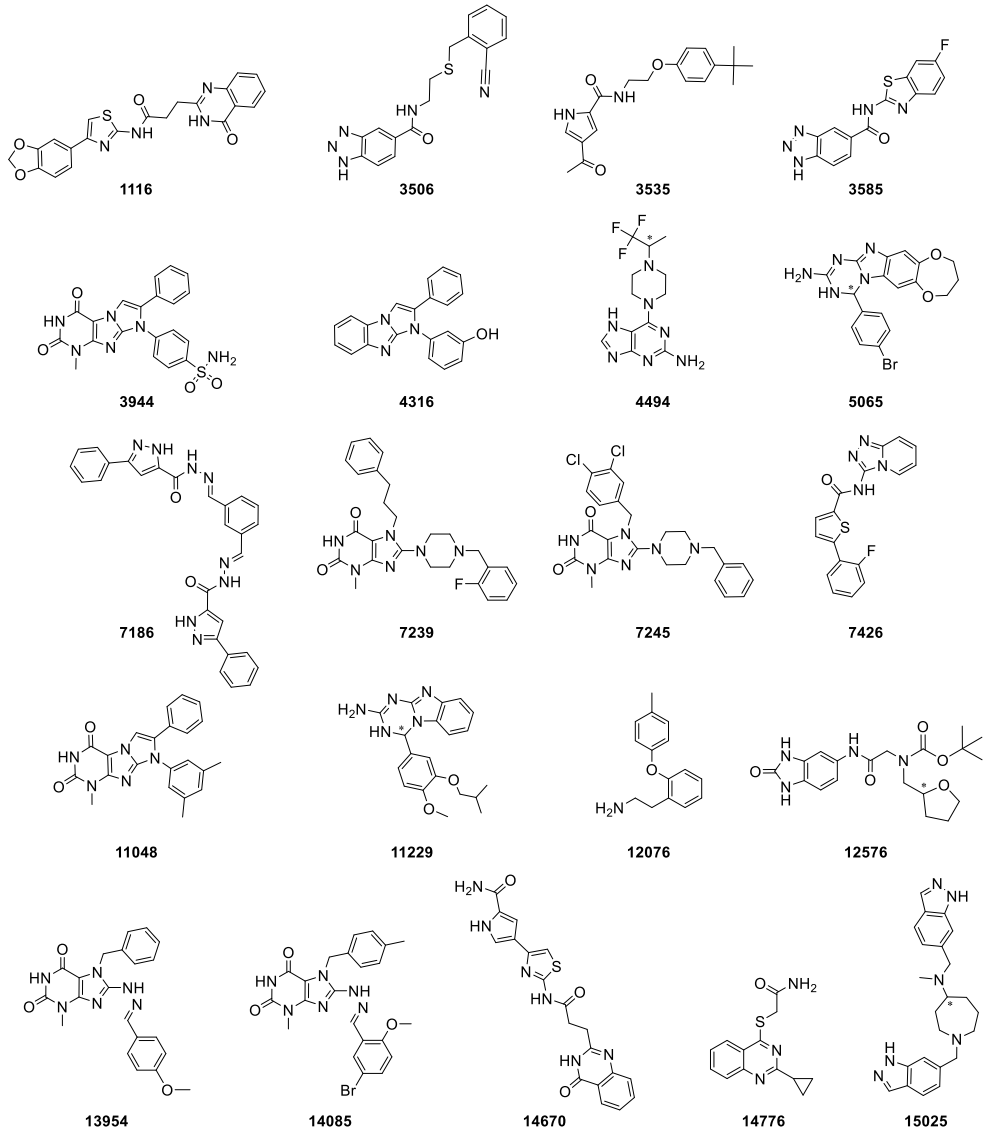

Figure S3.2. Molecular structures of most promising hits. * Denotes a chiral centre.

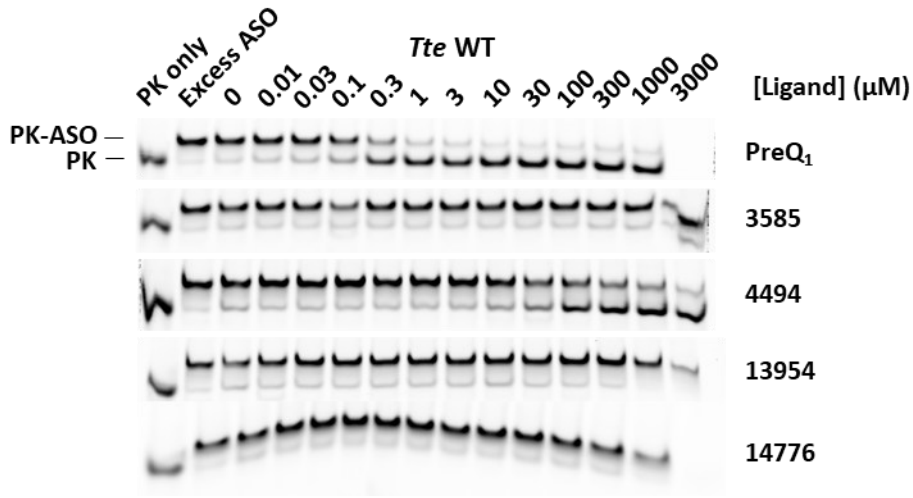

Figure S3.3. Competitive binding antisense assay (CB ASsay) with the *Thermoanaerobacter tengcongensis* (*Tte)* riboswitch visualized on native PAGE. Cy5-PK (1 eq.) was pre-incubated with a ligand, after which unlabelled antisense oligonucleotide (ASO) (1 eq.) was added, and the two possible conformations (PK and PK-ASO) were separated on a 20% (w/v) polyacrylamide gel.

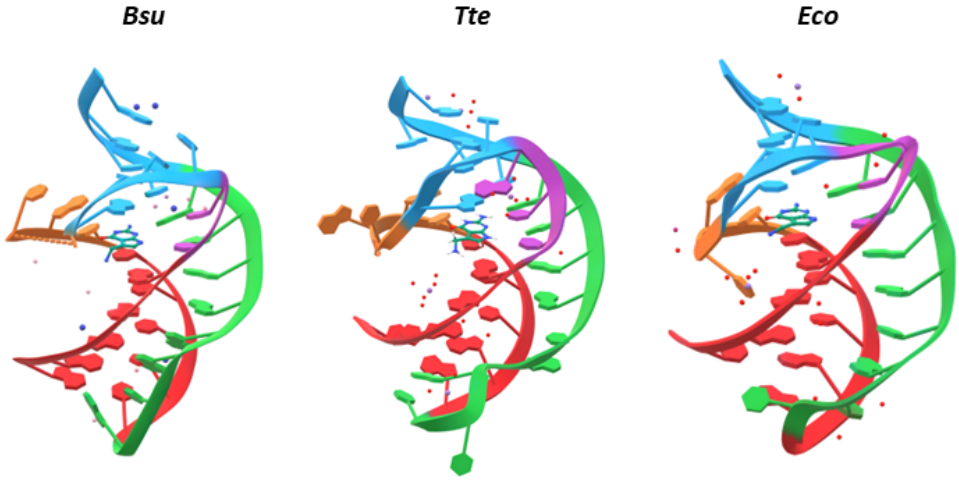

Figure S3.4. Published crystal structures of the *Bacillus subtilis* (*Bsu*) (PBD: 3FU2), *Thermoanaerobacter tengcongensis* (*Tte*) (PDB: 6VUI) and *Escherichia coli* (*Eco*) (PDB: 8FZA) $PreQ_1$ riboswitches, co-crystallized with $PreQ_1$.

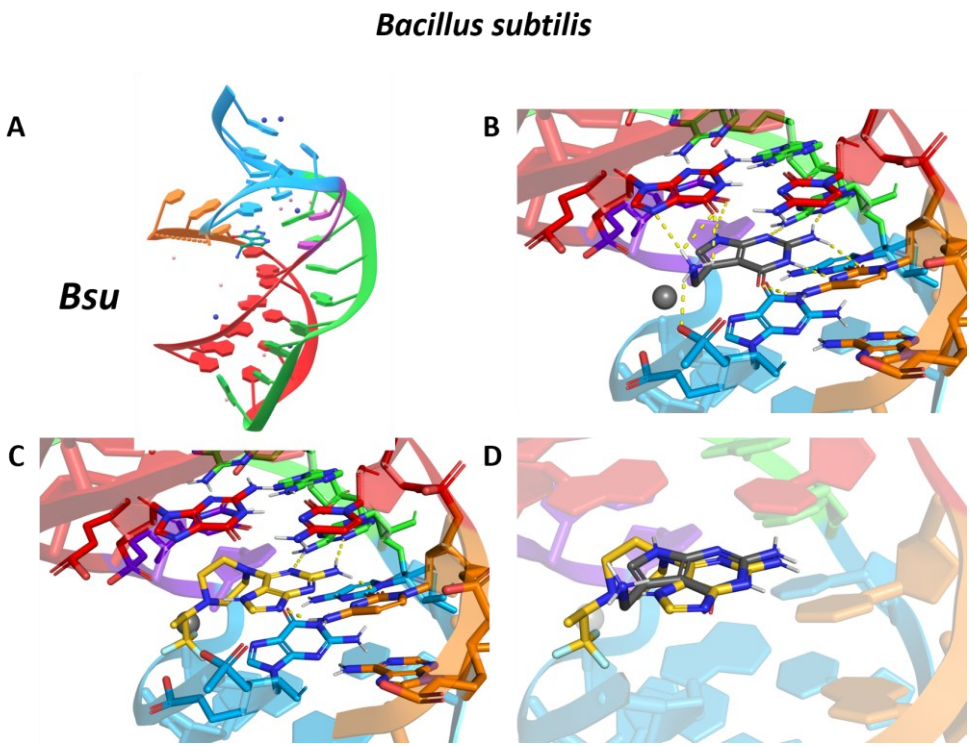

Figure S3.5. Docking of $PreQ_1$ and **4494** to the *Bacillus subtilis* (*Bsu*) $PreQ_1$ riboswitch (PDB ID: 3FU2). Most probable binding pose of **4494** was manually selected. Hydrogen bonds are indicated with yellow dashed lines. **A)** Crystal structure of the *Bsu* $PreQ_1$ riboswitch co-crystallized with $PreQ_1$. **B-C)** Close up docked structure of $PreQ_1$ (**B**) or **4494** (**C**) bound to the *Bsu* $PreQ_1$ riboswitch. **D**) Superimposed binding poses of $PreQ_1$ and **4494** to the riboswitch.

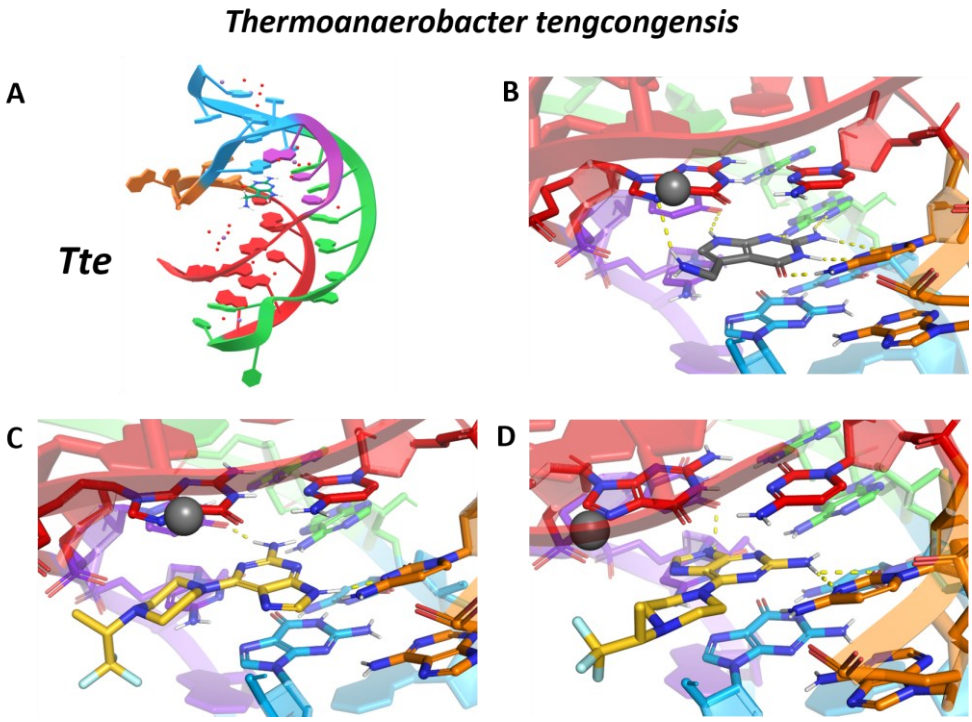

Figure S3.6. Docking of $PreQ_1$ and **4494** to the *Thermoanaerobacter tengcongensis* (*Tte*) $PreQ_1$ riboswitch (PDB ID: 6VUI). Most probable binding pose of **4494** was manually selected. Hydrogen bonds are indicated with yellow dashed lines. **A)** Crystal structure of the *Tte* $PreQ_1$ riboswitch co-crystallized with $PreQ_1$. **B-D)** Close up docked structure of $PreQ_1$ (**B**) or **4494** (**C** and **D**) bound to the *Tte* $PreQ_1$ riboswitch.

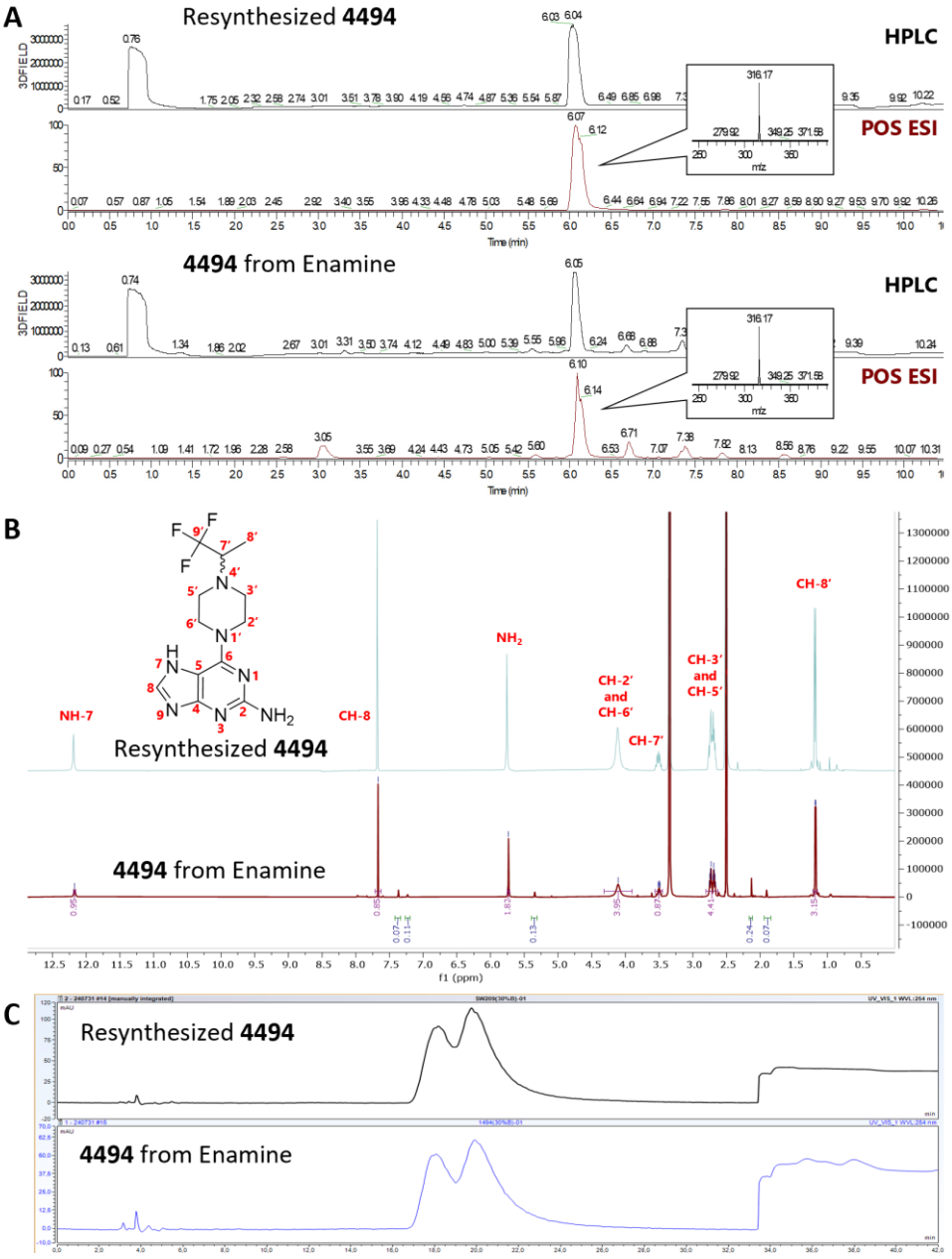

Figure S3.7. A) LCMS of resynthesized **4494** and **4494** from Enamine (H_2O+0.1% TFA to 50% acetonitrile in H_2O+0.1% TFA), with UV-Vis trace ('HPLC') and mass spectrum ('POS ESI') ranging from m/z 100-1000. Specific mass of the main compound (m/z = 316.17) is shown in the zoom. **B)** NMR of resynthesized **4494** and **4494** from Enamine in DMSO-d_6. Molecular structure of **4494** is indicated, and assignments are shown in red. **C)** Chiral column of resynthesized **4494** and **4494** from Enamine (7% isopropyl alcohol in n-heptane supplemented with 0.035% diethylamine).

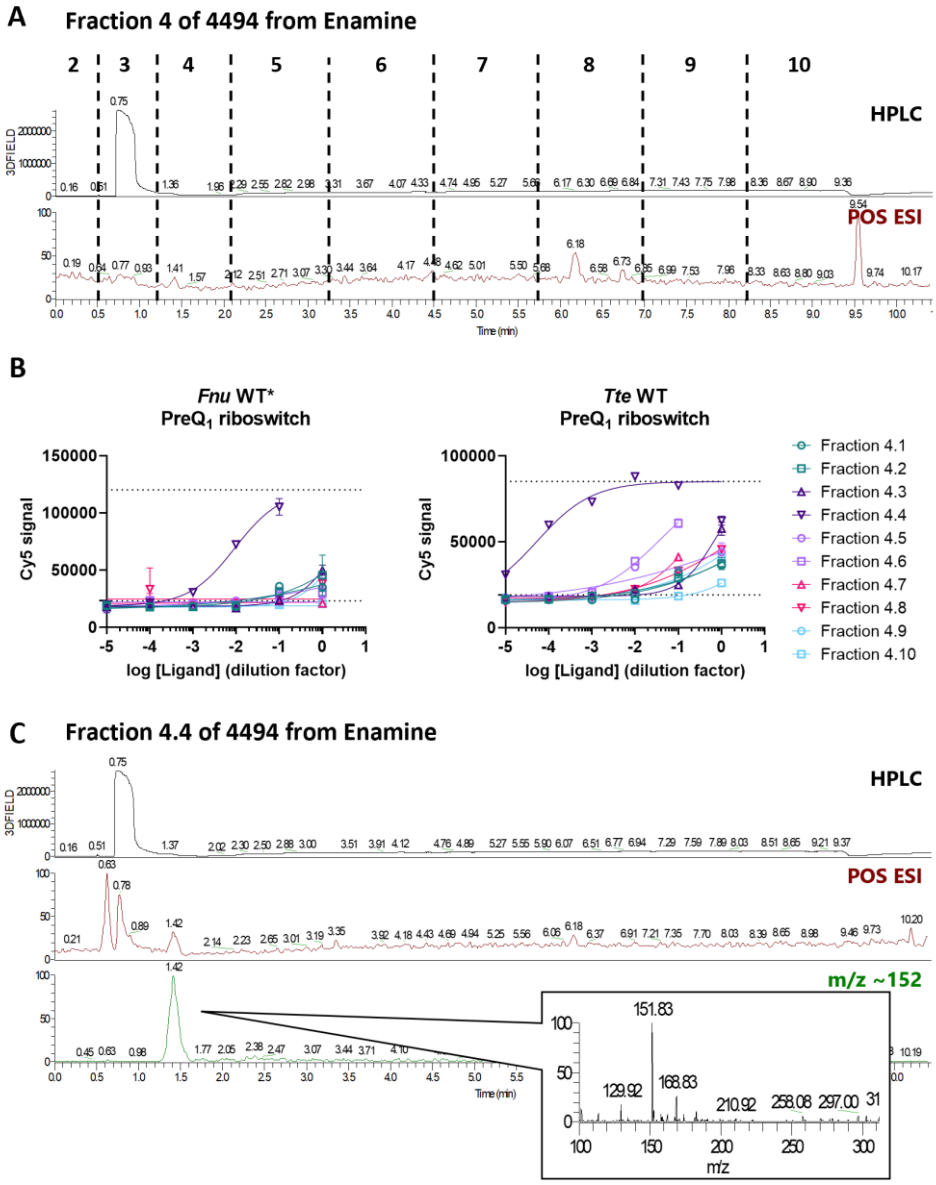

Figure S3.8. Analysis of **4494** from Enamine. **A)** LCMS of Fraction 4 of **4494** from Enamine (H_2O+0.1% TFA to 50% acetonitrile in H_2O+0.1% TFA), with UV-Vis trace ('HPLC') and mass spectrum ('POS ESI') ranging from m/z 100-1000. Indicated with dashed lines are the fractions collected with preparative HPLC. **B)** Competitive binding antisense assay (CB ASsay) of fractions 4.1 - 4.10 of **4494** from Enamine for the wildtype* (WT*) $PreQ_1$-I riboswitches of *Fusobacterium nucleatum* (*Fnu*) (left) and WT *Thermoanaerobacter tengcongensis* (*Tte*) (right). Dotted lines denote the minimum and maximum Cy5 signal as determined by the positive and negative controls. **C)** LCMS of Fraction 4.4 of **4494** from Enamine (H_2O+0.1% TFA to 50% acetonitrile in H_2O+0.1% TFA), with UV-Vis trace ('HPLC'), mass spectrum ('POS ESI') ranging from m/z 100-1000 and the occurrence of mass range 151-153 ('m/z ~152'). Specific mass of the enriched impurity (m/z = 151.83) is shown in the zoom.

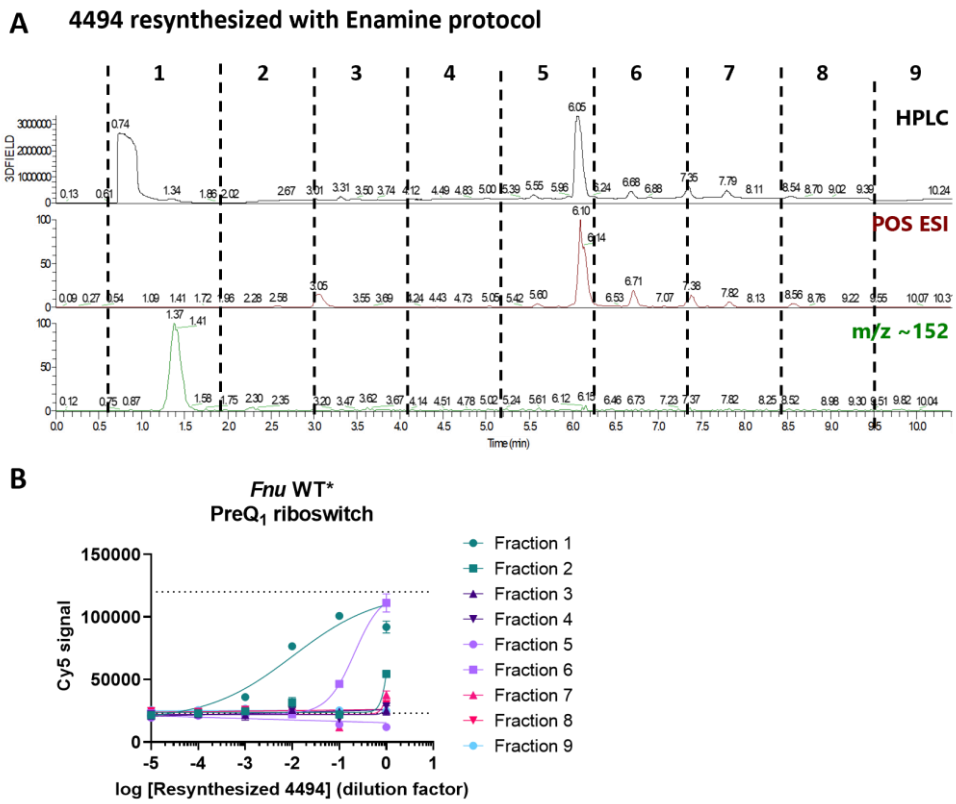

Figure S3.9. A) LCMS of **4494** resynthesized with the Enamine protocol (H_2O+0.1% TFA to 50% acetonitrile in H_2O+0.1% TFA), with UV-Vis trace ('HPLC'), mass spectrum ('POS ESI') ranging from m/z 100-1000 and the occurrence of mass range 151-153 ('m/z ~152'). Indicated with dashed lines are the fractions collected with preparative HPLC. **B)** Competitive binding antisense assay (CB ASsay) of fractions 1 - 9 of **4494** resynthesized with the Enamine protocol for the wildtype* (WT*) $PreQ_1$-I riboswitch of *Fusobacterium nucleatum* (*Fnu*). Dotted lines denote the minimum and maximum Cy5 signal as determined by the positive and negative controls.

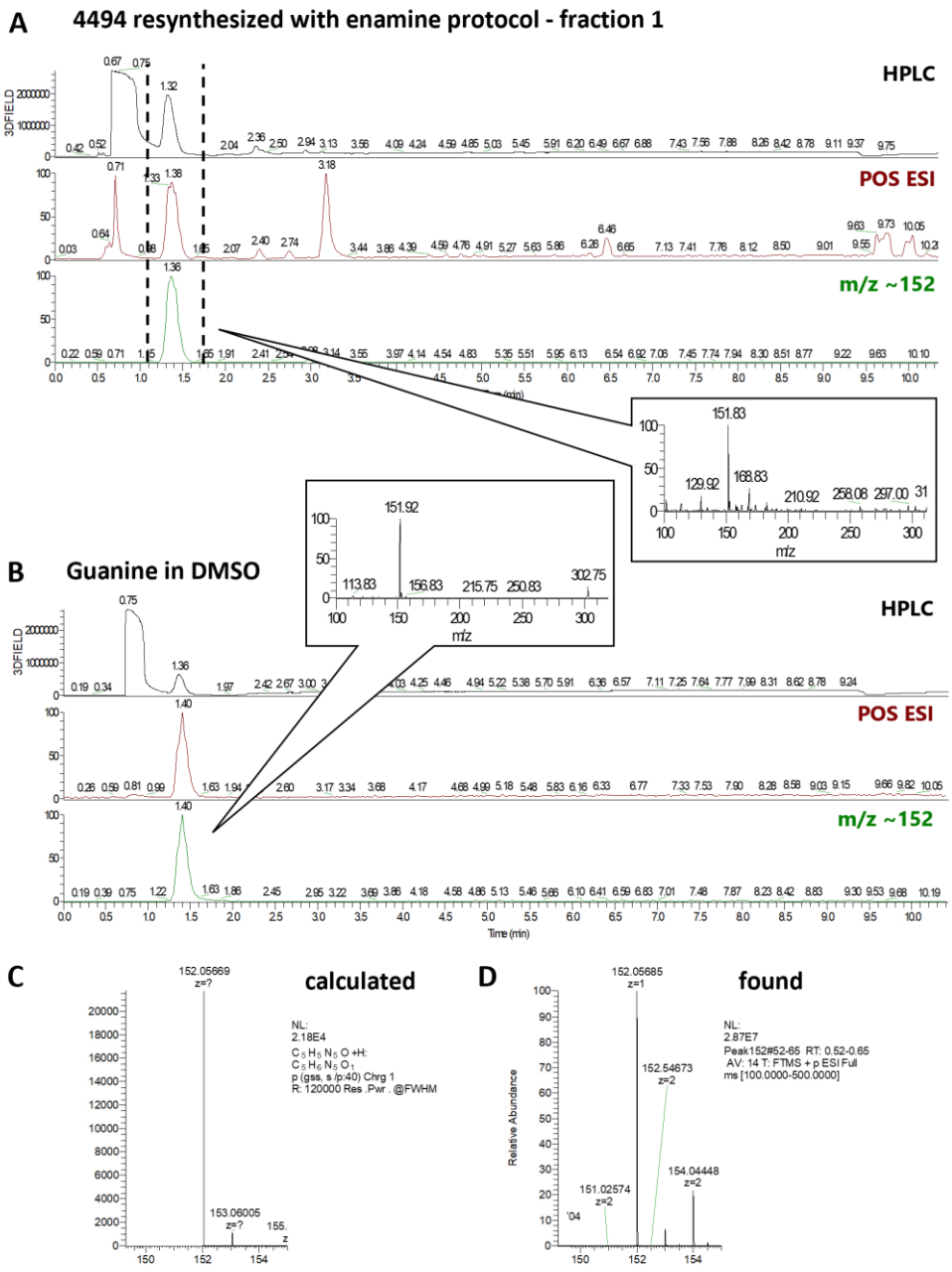

Figure S3.10. A-B) LCMS of Fraction 1 of **4494** resynthesized with the Enamine protocol (**A**) and Guanine (**B**) (H_2O+0.1% TFA to 50% acetonitrile in H_2O+0.1% TFA), with UV-Vis trace ('HPLC'), mass spectrum ('POS ESI') ranging from m/z 100-1000 and the occurrence of mass range 151-153 ('m/z ~152'). Indicated with dashed lines is the fraction collected with preparative HPLC. Specific masses of the enriched impurity (m/z = 151.83) and Guanine (m/z = 151.92) are shown in the zoom. **C-D)** HRMS of Fraction 1 of **4494** resynthesized with the Enamine protocol. Calcd. for $[C_5H_6N_5O]^+$ 152.05669 (**C**); found 152.05685 (**D**).

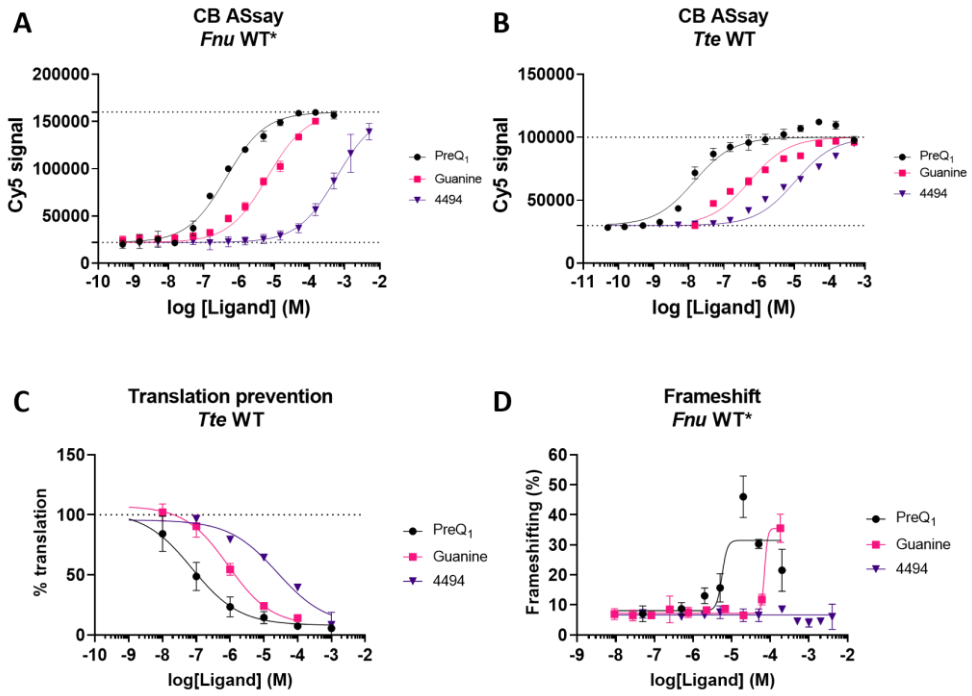

Figure S3.11. Comparison of $PreQ_1$, Guanine and **4494** from Enamine. **A-B)** Competitive binding antisense assay (CB ASsay) for the wildtype* (WT*) $PreQ_1$-I riboswitch of *Fusobacterium nucleatum* (*Fnu*) (**A**) and WT *Thermoanaerobacter tengcongensis* (*Tte*) (**B**). Dotted lines denote the minimum and maximum Cy5 signal as determined by the positive and negative controls. **C)** Translation prevention assay with the *Tte* $PreQ_1$ riboswitch. Translation percentages were calculated by normalizing the luminescence signal to the DMSO control. Measurements were performed in duplicate. **D)** Frameshift assays with the WT* *Fnu* $PreQ_1$ riboswitch. Frameshift percentages were calculated by normalizing the luminescence signal to the in-frame control. Measurements were performed in duplicate.

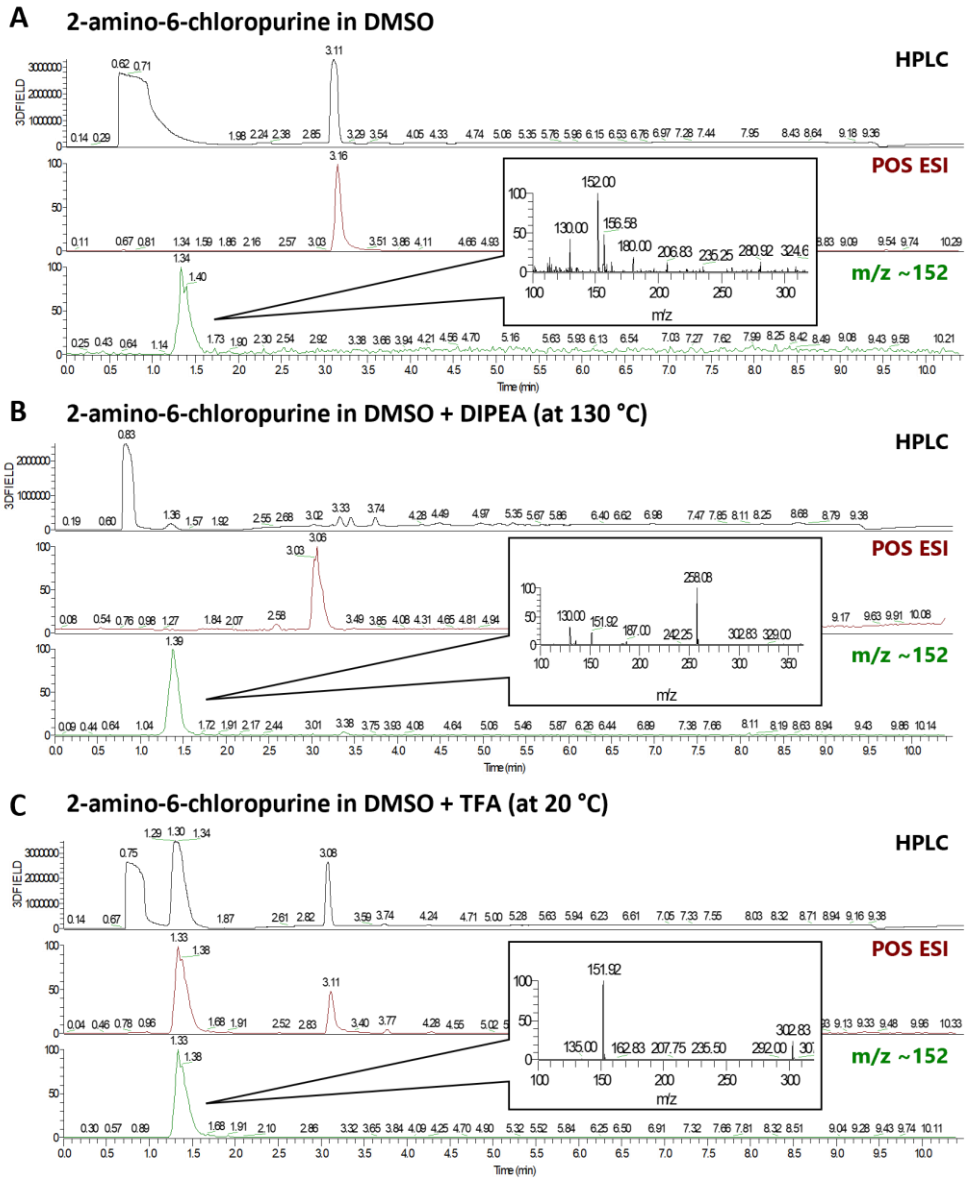

Figure S3.12. A) LCMS of 2-amino-6-chloropurine in DMSO. **B)** LCMS of 2-amino-6-chloropurine in DMSO + DIPEA stirred at 130 °C. **C)** LCMS of 2-amino-6-chloropurine in DMSO + TFA stirred at 20 °C. All samples were analysed using H_2O+0.1% TFA to 50% acetonitrile in H_2O+0.1% TFA, with UV-Vis trace ('HPLC'), mass spectrum ('POS ESI') ranging from m/z 100-1000 and the occurrence of mass range 151-153 ('m/z ~152'). Specific masses of the enriched impurity (m/z ≈ 152) are shown in the zoom.